Francisco Ribeiro Ferreira

Licenciatura em Ciências de Engenharia Biomédica

Chitosan Nanoparticles as Drug Delivery Systems

Dissertação para obtenção do Grau de Mestre em
Engenharia Biomédica

Orientador: Prof.Doutor João Paulo Borges,Professor Auxiliar,DCM-FCT/UNL

Co-orientador: Doutora Paula Pereira Soares, DCM-FCT/UNL

Júri:

Presidente: Doutora Carla Maria Quintão Pereira, Professora Auxiliar,FCT/UNL

Arguentes: Doutora Célia Maria Reis Henriques, Professora Auxiliar, FCT/UNL

Vogais: Doutor João Paulo Borges, Professor Auxiliar, FCT/UNL

FACULDADE DE CIÊNCIAS E TECNOLOGIA
UNIVERSIDADE NOVA DE LISBOA

Novembro, 2015

Francisco Ribeiro Ferreira

Licenciatura em Ciências de Engenharia Biomédica

Chitosan Nanoparticles as Drug Delivery Systems

Dissertação para obtenção do Grau de Mestre em
Engenharia Biomédica

Orientador: Prof. Doutor João Paulo Borges, Professor Auxiliar, DCM-FCT/UNL

Co-orientador: Doutora Paula Pereira Soares, DCM-FCT/UNL

Chitosan Nanoparticles as Drug Delivery Systems

"Every person must work for his own improvement, and at the same time he must share a general responsibility for all humanity"

Marie Curie

"A person who never made a mistake never tried anything new"

Albert Einstein

Acknowledgments

First of all I want to thank to all my friends that I met in these years and that share with me the excellent experience that was study in FCT-UNL. Without them, all the classes and study seasons wouldn't be the same. An especial thank to the ones that lived with me in Frausto da Silva residence. It wouldn't be possible to complete my graduation without all of them.

I would like to thank all the support given by the members of the Biomaterials Group, Professors, Post-Doc, PhD and Master's students that share with me all the knowledge and made my thesis experience much more interesting.

A special thanks to my "chefinha" Paula Soares for all the patience and knowledge that she shared with me. She was always available to help me.

I would like to express my gratitude to Prof. João Paulo Borges, my supervisor in this adventure, for the opportunity of being part of the Biomaterials Group and to give me the chance to share with me his knowledge in the biomaterials area.

I want to thank to Prof. Jorge Silva for all the knowledge, help and for providing the opportunity to use his laboratory for the *in vitro* cell viability and proliferation studies.

For the encouragement and motivation to finish my thesis, I want to thank to my work colleagues and managers.

Finally, I want to thank to my family for being my support in this journey and in my life. I am who I am because of their education and life's experience.

Abstract

The goal of the present work is to synthesize chitosan-coated superparamagnetic iron oxide nanoparticles (CS SPIONs) for doxorubicin (DOX) delivery for cancer theranostics. The CS SPIONs will be loaded with the anticancer drug DOX because it is largely used clinically for different cancers types. In this work chitosan nanoparticles (CS NPs) and iron oxide nanoparticles were synthetized by ionic gelation and thermal decomposition techniques, respectively. Chitosan depolymerization was performed to be used different molecular weights (474 – 39 kDa) to produce CS NPs with different diameters. Magnetic stirring and pH influence were also studied. Dynamic Light Scattering (DLS) measurements indicate that was obtained different nanoparticles diameters, approximately the lowest diameters were around 100 nm and 9 nm for CS NPS and iron NPs respectively. Then, CS SPIONs were formed. Synthetized nanoparticles were characterized by (DLS), UV-Visible (UV-Vis), Fourier Transform Infrared Spectroscopy (FTIR) and Transmission Electrons Microscopy (TEM). Superconducting Quantum Interference Device (SQUID) and magnetic hyperthermia studies indicate that this nanoparticles show a superparamagnetic behavior and the ability to generate heat. These characteristics are essential to be possible to use these nanoparticles in biomedical applications such as contrast agents for MRI, magnetic drug delivery, cancer diagnostics and treatment. The DOX delivery studies indicate that the drug release depends on pH and in the first 10-20 hours the majority of drug is released. Finally, the *in vitro* cell viability and proliferation studies were conducted using the Vero cell line. These studies indicate that the CS SPIONs synthetized in the present work are non-toxic up to the CS SPIONs concentration of 1.25 mg/ml. Considering all the studies conducted in this work, it can be concluded that the nanoparticles synthetized possess the necessary characteristics to be used in biomedical applications.

Keywords:

Chitosan, Iron Oxide, Nanoparticles, Doxorubicin, Drug Delivery Systems

Resumo

O objectivo do presente trabalho é sintetizar nanopartículas de óxido de ferro revestidas com quitosano (CS SPIONs) para libertação de doxorubicina (DOX) para teragnóstico de cancro. Estas nanopartículas irão encapsular este farmáco anticancerígeno pois é frequentemente utilizado para diferentes tipos de cancro. Neste trabalho foram produzidas nanopartículas de quitosano (CS NPs) e de óxido de ferro pela técnica de gelação iónica e decomposição térmica respetivamente. Procedeu-se à despolimerização do quitosano para serem usados diferentes pesos moleculares (474 a 39 kDa) de forma a se poder produzir nanopartículas com diferentes diâmetros. A influência da agitação magnética e do pH foram também estudados. As medições de DLS indicam que foram obtidos diferentes diâmetros para as nanopartículas, sendo os diâmetros mais pequenos de aproximadamente 100 e 9 nm para as nanopartículas de quitosano e de óxido de ferro respetivamente. Posteriormente, foram sintetizadas CS SPIONs. As nanoparticulas sintetizadas foram caracterizadas por DLS, UV-Vis, FTIR e TEM. Os estudos magnéticos de hipertermia e SQUID indicam que as nanopartículas apresentam um comportamento de superparamagnetismo e capacidade de gerar calor. Estas características são essenciais para que as nanopartículas possam ser utilizadas em aplicações biomédicas como agentes de contraste para MRI, libertação magnética de fármaco, diagnóstico e tratamento de cancro. Os estudos de libertação da DOX mostram que a libertação depende do pH e a mesma é feita na sua maioria nas primeiras 10-20 horas. Finalmente, os estudos *in vitro* de viabilidade e proliferação celular, realizados usando a linha celular Vero, mostram que as CS SPIONs produzidas não são citotóxicas até uma concentração de CS SPIONs de 1,25 mg/ml. Considerando todos os estudos realizados neste trabalho pode-se concluir que as nanopartículas produzidas possuem as características necessárias para serem utilizadas em aplicações biomédicas.

Palavras-chave:

Quitosano, Óxido de Ferro, Nanopartículas, Doxorubicina, Sistemas de Libertação de Fármaco

Contents

List of Tables

List of Figures

Abbreviations and Acronyms

ASTM: American Society for Testing Materials

CS: Chitosan

CS M_v: Chitosan Molecular Weight

CS NPs: Chitosan nanoparticles

DLS: Dynamic Light Scattering

DMEM: Dulbecco's Modified Eagle Medium

DMSO: Dimethyl Sulfoxide

DOX: Doxorubicin

FC: Field-cooled

FTIR: Fourier Transform Infrared Spectroscopy

ISO: International Organization of Standardization

M_S: Saturation magnetization

MRI: Magnetic Resonance Image

NP: Nanoparticle

PBS: Phosphate Buffered Saline

SCENIHR: Scientific Committee on Emerging and Newly Identified Health Risks

SPIONs: Superparamagnetic iron oxide nanoparticles

SQUID: Superconducting Quantum Interference Device

SSA: Specific Surface Area

TEM: Transmission Electrons Microscopy

TPP: Tripolyphosphate

TREG: Triethlylene Glycol

UV-Vis: UV-Visible

XRD: X-Ray Diffraction

ZFC: Zero-field-cooled

1. INTRODUCTION

1.1. Motivation and Objectives

Chitosan-coated iron oxide nanoparticles have been widely investigated because of its potential biomedical applications such as in magnetic resonance image (MRI), magnetic drug delivery, cancer diagnostics and treatment.

The big challenge in cancer therapy is minimizing side effects and maximizing efficacy. To solve the reducing sensitivity of tumor cells to cytotoxic drugs [1], different biodegradable materials are being used in the cancer therapeutic systems.

In order to improve patient care and quality of life, it is necessary reduce off-target toxicities by directing anticancer drugs (e.g. doxorubicin) to intracellular targets of tumor cells [2]. It is probably possible by using chitosan-coated SPIONs approaches to drug delivery because magnetic nanoparticles seem to be the most promising materials [1].

In order to achieve a carrier that is biocompatible and biodegradable, the goal of this thesis is to synthesize chitosan-coated superparamagnetic iron oxide nanoparticles for doxorubicin delivery for cancer theranostics. The chitosan-coated SPIONs will be loaded with the anticancer drug doxorubicin (DOX) because it is largely used clinically for different cancers types.

1.2. Thesis Overview

This thesis is divided in 4 parts: Introduction, Materials and Methods, Results and Discussion, and Conclusions.

In the first part, it is described the *state of the art* about the production of chitosan nanoparticles and its applications as well as the production and biomedical applications of iron oxide nanoparticles. It is also described the anticancer drug doxorubicin and its effects. In Materials and Methods are presented the protocols followed to synthesize chitosan and iron oxide nanoparticles as well as all the others protocols used to perform laboratory work. The results of laboratory work are presented and discussed in Results and Discussion section. Finally, possible conclusions to be drawn from the work are presented in the last section.

2. NANOTECNOLOGY, NANOMATERIALS, AND NANOPARTICLES

Nanotechnology is an interdisciplinary area that involves chemistry, physics, biology, engineering sciences and technology. Nanotechnology allows the development of several biomedical applications such as diagnostic devices, contrast agents for magnetic resonance imaging (MRI), and drug delivery systems, for instance, anticancer drugs, proteins, and genes [3, 4].

Current nanoparticle (NP) definition is complex and not consensual because only takes into account the particle size. For instance, ISO, International Organization of Standardization, states that NP is a particle with all three dimensions from 1 to 100 nm, while ASTM, American Society for Testing Materials, and SCENIHR, Scientific Committee on Emerging and Newly Identified Health Risks, defend that NP is a particle with only two (or three) dimensions from 1 to 100nm [4-6]. On the other hand, some authors consider that nanoscale is not only from 1 to 100 nm, but from 1 to 999 nm, therefore they defend that NP is a particle with its dimensions in a size range from 1 to 999 nm [4].

However, none of those definitions take into account how properties may change with the size. In order to achieve a better definition, the European Commission considers that the size should not be the only criteria to categorize nanomaterials and NPs, so defined the other criteria to categorize them such as size distribution, specific surface area (SSA), surface modifications, and other physical properties [4-6].

2.1. Superparamagnetic Iron Oxide Nanoparticles - SPIONS

In recent years, superparamagnetic iron oxide nanoparticles (SPIONs) have been widely studied because of its potential biomedical applications such as contrast agents for MRI, magnetic drug delivery, cancer diagnostics and treatment [7, 8]. Currently, as is shown in table 2.1, several nanoparticles are already used clinically.

In addition to those, SPIONs offer other applications such as magnetic guidance and magnetic fluid hyperthermia [8]. Hyperthermia is a type of cancer treatment in which body tissue is exposed to high temperatures (40ºC-45°C) to damage and kill cancer cells, without using drugs or radiation, when placed in an oscillating magnetic field. The magnetic field can penetrate deep in living tissues without being absorbed by them. Side effects are reduced because cancer cells are more sensitive to temperature oscillations then normal cells. This property allows its application in the treatment of tumors and in drug delivery [4]. The above cited properties of SPIONs offer the possibility of using these nanoparticles both in medical diagnostic and therapeutic (*theranostics*) [9, 10].

Table 2.1- SPIONs approved to be used clinically in USA, Europe and their applications

	USA	Europe	Applications
Ferumoxides	Feridex® [11, 12]	Endorem® [13-15]	MR imaging to detect and characterize focal liver lesions
Ferucarbotran	Resovist™ [12, 16]	Resovist™	Liver imaging and diagnostics of benign and malignant lesions
	Combidex® [15, 17, 18]	Sinerem™ [19, 20]	Detect metastatic lymph nodes in MRI and liver imaging
Ferumoxytol [21-23]	Feraheme [24]	Rienso® [25]	Prostate cancer; functional brain activation; iron-deficiency anemia in adults with chronic kidney disease

Despite these advantages the medical use of SPIONs possess some challenges, such as the disappearance from the bloodflow in a few minutes after their intravenous injection, the lack of surface functional groups and the need to obtain hydrodynamic stability under biological conditions such as temperature and ionic concentration [8]. A solution for those problems could be masking SPIONs' surface charges and coating the particles with hydrophilic polymers.

2.1.1. Synthesis of SPIONs

There are numerous methods to synthesize superparamagnetic iron oxide nanoparticles such as micro emulsion, chemical precipitation and high temperature reactions [26].

(i) Micro emulsion

Micro emulsion is related to a mixture of the following three components: an oil phase, an aqueous phase and the third component called surfactant. The dispersed droplets, obtained by this technique, possess a diameter between 10-300 nm [27].

Surfactant are molecules with one part soluble in polar solvents, known as hydrophilic and called head, and the other part insoluble in the same polar solvents, known as hydrophobic and called tail. This characteristic gives to surfactant molecule some capabilities such as the ability to adsorb at the surfaces and interfaces which results in the formation of micro emulsions due to the decrease of surface tension and also the formation of aggregates inside the solution. These aggregates can solubilize oil droplets

into an aqueous phase, called micelles, or water in the oily phase, known as reversed micelles. Surfactants can be obtained from synthetic or natural resources and can be simple molecules such as sodium or potassium salt of the carboxylic acids, or polymers with various molecular weights. Several functional groups can be used as head groups such as carboxylates, sulphates, phosphates, sulfonates, quaternary amines and polyethers.

This method produces monodispersed iron oxide nanoparticles, presenting a high control of its distribution size [28], smaller and uniform when compared to others methods [29]. Although these advantages, some disadvantages are important to enunciate, such as organic solvents toxicity which affects the usage of these nanoparticles in biomedical applications. Besides that, the amount of oil required and the difficulty of surfactant molecules removal from the nanoparticles makes this method difficult to dimension [28].

(ii) Chemical Precipitation

Chemical precipitation is a simple and efficient chemical pathway to produce SPIONs. This method allows us to produce large quantities of SPIONs. These nanoparticles are prepared by co-precipitating Fe (III) and Fe (II) in an aqueous medium. The reaction can be written as:

$$Fe^{2+} + 2Fe^{3+} + 8OH^- \rightarrow Fe_3O_4 + 4H_2O \quad \textbf{Eq. 1}$$

Physical and chemical properties of SPIONs can be affected by ions oxidation. To avoid oxidation, this reaction must be done under nitrogen environment.

Although chemical precipitation is a simple and efficient method, it exhibits some disadvantages such as the difficulty to control particle size and size distribution. Therefore, several studies were made to adjust different factors that affect the size and size distribution such as ionic strength, pH, temperature, and Fe^{3+}/Fe^{2+} ratio [26].

(iii) High Temperatures Reactions

Thermal decomposition method is a technique to produce high-quality superparamagnetic and monodisperse magnetite nanoparticles by the decomposition of the iron acetylacetonate, $Fe(acac)_3$, in a high-boiling temperature solvent with surfactants such as oleic acid and oleylamine [30].

However, thermal decomposition method to directly produce water-soluble magnetic nanoparticles was developed by polyol-mediated synthesis. High-boiling solvents are required to achieve high temperatures (200-300ºC) for decomposition of the iron acetylacetonate, $Fe(acac)_3$, such as ethylene glycol, triethlylene glycol (TREG), tetraethylene glycol (TEG), poly-(ethylene glycol) (PEG), and poly(vinyl alcohol) (PVA) or 2-pyrrolidone [31]. TREG is used in these reactions not only as a solvent but also as a reducing agent and stabilizer to control the particle growth and prevent aggregation.

With this method we can directly synthesize water-soluble SPIONs [30, 31]. SPIONs produced by this technique show a hydrophilic coating, acceptable size uniformity, and good crystallinity, thus offering powerful potential for biomedical applications such as the ability of TREG-coated SPIONs to act as superparamagnetic contrast agents in MRI or as agents for magnetic hyperthermia [31].

These SPIONs are biocompatible up to an iron concentration of 80µg/ml with SiHa, B16F10 and mouse primary fibroblast cells. The significant temperature rise (RF radiation with 20 MHz frequency and 100 W power) from 31-49ºC in 275 seconds for a sample with iron concentration of 0.5 mg/ml and from 35-70ºC in 150 seconds for 1 mg/ml, corroborates their applicability for magnetic hyperthermia application [30].

2.2. Chitosan Nanoparticles – CS NPs

Chitosan is a natural polysaccharide composed of D-glucosamine and N-acetyl-D-glucosamine units linked by β-(1,4)-glycosidic bonds. It is obtained by partial deacetylation of chitin, the second most abundant polymer in nature. Chitin and chitosan differ in the molar fraction of the deacetylated units (DD in figure 2.1). The DD is responsible for the different physic-chemical properties of these polymers. Chitosan is the polymer with a DD higher than 0.5 (typically 0.7-0.8) soluble in acidic solutions. Chitin is almost insoluble in most organic solvents and because of its low solubility, chitin has limited applications. On the contrary chitosan is soluble in acidic solutions due to protonation of the amine groups ($-NH_2$) of the D-glucosamine unit, where CS is converted to a cationic polyelectrolyte, and possess a great affinity to form films, gels, and fibers used in different applications [32, 33].

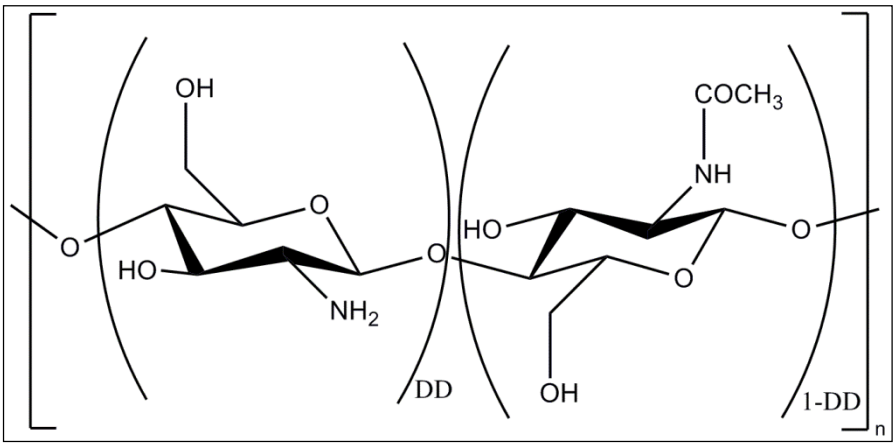

Figure 2.1- Chemical structure of chitosan

This polymer is nontoxic, biocompatible and biodegradable, and along with nanoparticles has been utilized as a stabilizing agent because of its film-forming ability, mechanical strength, high permeability towards water, susceptibility to chemical modifications, cost-effectiveness [3].

Chitosan nanoparticles (CS NPs) possess interesting biomedical applications. They can be used as carriers in controlled drug delivery of:

(i) doxorubicin - an anticancer drug used for the treatment of several tumors [34, 35];

(ii) 5-fluorouracil (5-FU) and leucovorin (LV) - drugs used in the treatment of colon cancer [36];

(iii) avidin and biotin – drugs used for hepatic carcinoma treatment [37], among others.

CS NPs have been also studied in: gene delivery systems [38, 39]; siRNA delivery [40]; release of vitamin C [41]; delivery of pDNA against hepatitis B through nasal mucosa [42]; protein delivery systems [43], such as insulin [44] or BSA [45] delivery; release of polyphenolic antioxidants , for instance, catechins in gastrointestinal track (GIT) [46-48]; and as supports for enzyme immobilization [49]. CS NPs could also inhibit the growth of several microorganisms and possess , in some cases, higher antibacterial activity than CS itself [50].

2.2.1. Synthesis of CS NPs

There are several techniques to synthesize CS NPs such as micro emulsion, electrospray, emulsification solvent diffusion, and ionic gelation [51].

(i) Micro emulsion

Micro emulsion method was first developed by Maitra and his coworkers [52]. This technique consists in the conjugation of the functional amine group of CS with aldehyde groups of the cross-linking agent, such as glutaraldehyde. In this method, CS nanoparticles are formed by adding, under stirring, chitosan solution with glutaraldehyde to a mixture that contains a surfactant dissolved in N-hexane. The organic solvent and the excess surfactant are removed, and the nanoparticles suspension is dialyzed and finally lyophilized.

This method allows control the particle size by using different amounts of cross-linked agent glutaraldehyde. However, micro emulsion exhibits some disadvantages such as the use of organic solvents, lengthy preparation process, and it requires a complex washing step [52, 53].

(ii) Electrospray

Electrospray method consists in a modification of electrospinning technique that is a widely used technique to produce micro/nanofibers. Electrospray process consists in applying a high voltage to a polymeric solution that allows the emission of droplets from the solution cone that became dried before reaching the target and forming these way solid nanoparticles. The advantages of electrospray are the

narrow size distribution, simplicity, and fast preparation. However, there are a few studies using this technique to produce nanoparticles [54].

(iii) Emulsification Solvent Diffusion

Originally developed by Niwa and his team with PLGA, El-Shabouri (2002) used this technique to prepare chitosan nanoparticles. This method consists in an oil-in-water (o/w) emulsion obtained by injecting an organic solvent into a chitosan solution with a stabilizing agent, such as polomaxer, under mechanical stirring. Then, a large volume of water is added to the emulsion to overcome organic solvent miscibility in water. Nanoparticles are formed because of the diffusion of organic solvent into water that promotes polymer precipitation.

Emulsion solvent diffusion shows some disadvantages such as the use of organic solvents and high shear forces used to prepare nanoparticles [52].

(iv) Ionic Gelation

Ionic gelation technique was first reported by Calvo *et al*. (1997). This method consists in the addition of tripolyphosphate (TPP), a crosslinking agent, into the aqueous phase containing chitosan, thus leading to the formation of CS NPs [39]. In this work it was used ionic gelation technique with TPP because it is simple, mild, less toxic and suitable for scaling up [51]. Furthermore, it is possible to control the size of the CS NPs by adjusting the following parameters: CS and TPP concentration, CS/TPP weight ratio and volume ratio, pH value [51].

The formation of CS NPs by ionic gelation occurs in two steps. The first one is the addition of aqueous TPP solution to the previously dissolved CS in acidic solution. The second one is the spontaneously inter and intracrosslinking - gelation - between the protonated amine group on the CS molecules and TPP anions.

In order to achieve smaller NPs with narrower size distribution (low polydispersity) it is necessary a rapid mixing, which promotes a fast and uniform dispersion of the TPP anions within the CS chains [51].

2.2.2. Interaction between CS NPS and cells

The most relevant factors that affect the interaction between live cells and nanoparticles of polycationic polymers, where CS nanoparticles are included, are positive charge and nanoscale size [55]. The positive charge is an important factor because the proteins of the tight junction, Z0-1 and F-actin molecules, possess negative charge. Hence, positive charge is a relevant parameter for cell surface binding.

The effects of CS nanoparticles on the cells membrane are more intense than CS itself in some cases, but similar in others. Possibly, the effects are similar because both CS and CS nanoparticles are positive charged and they interact with negatively charged live cells by electrostatic forces by the same mechanism. On the other hand, the transformation of CS molecules into CS nanoparticles promotes the interaction because it changes the linear configuration of CS molecules, in microscale, to the condensed configuration of CS nanoparticles in nanoscale [55].

CS is considered non-cytotoxic and CS nanoparticles also exhibit no cytotoxicity although they accumulated more inside of the cells. There was no significant difference in cytotoxicity between both [55].

2.3. CS NPS as Delivery Systems for Doxorubicin

Doxorubicin is part of the family of anthracycline antibiotics. It is formed by an amino-sugar daunosamine, linked to the C7 of a tetracyclic aglycone, doxorubicinone [35, 56]. The chemical structure of doxorubicin is shown in Figure 2.2.

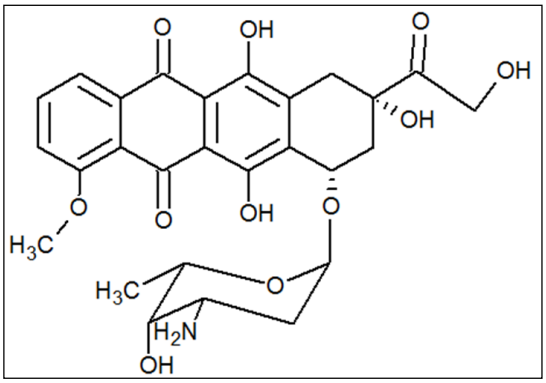

Figure 2.2- Chemical structure of Doxorubicin.

Doxorubicin is generally used in the treatment of several cancers such as acute leukemia, lymphomas, soft-tissue and osteogenic sarcomas, pediatric malignancies and adult solid tumors as breast and lung carcinomas. It is also used with other drugs such as methotrexate, cisplatin, ifosfamide, vincristine and etoposide [35].

However, only a small amount of DOX reaches the tumor target site because about 40% are excreted by liver metabolism. Furthermore, doxorubicin induces cardiac toxicity [34, 35, 56], but not in the same way to the different patients, for some started within 1 year of DOX therapy, while for others it occurred 15 years after the end of the treatment [35].

Doxil®, a liposomal form of DOX, was the first nano-drug approved by FDA in 1995 [57]. Doxil® is a liposomal drug delivery system clinically used to treat cancer, such as ovarian cancer. In comparison to free DOX, Doxil® liposomes have the ability to accumulate more amounts of drug in the

tumor sites by a phenomenon known as “Enhanced Permeability and Retention” (EPR) effect [58]. However, its efficacy is not consensual due to low response rates percentage in clinical trials and due to toxic dermatological reaction occurred in about 50 % of patients treated with Doxil® [35].

A solution to protect patients from DOX side effects is by using a drug delivery system compound by CS NPs. This way, and attending to CS properties, nontoxicity, biocompatibility and biodegradability, it is possible to encapsulate and delivery DOX with reduced side effects [35]. Figure 2.3 shows the mechanism of SPIONs encapsulation by CS.

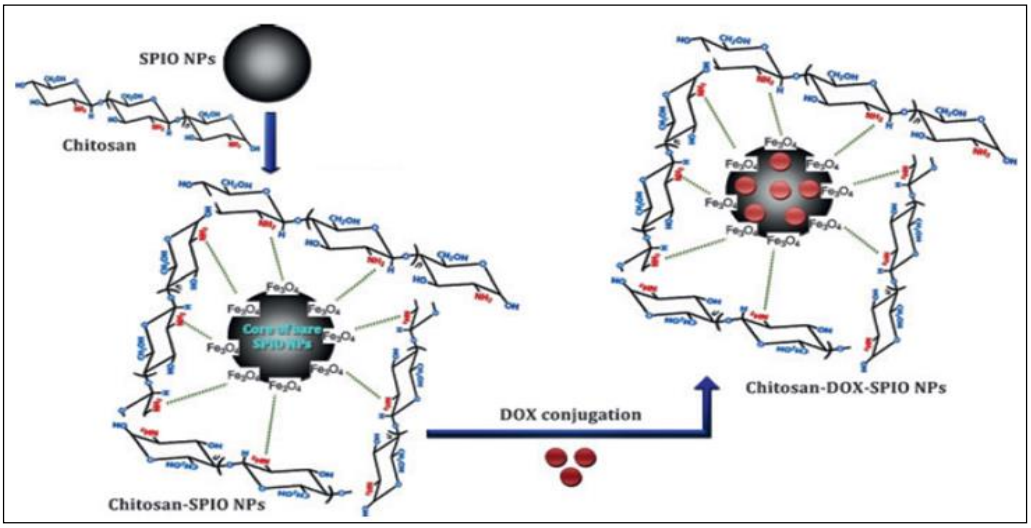

Figure 2.3- Adapted illustration of the modification mechanism of SPIONs with chitosan, followed by doxorubicin loading [1].

3. MATERIALS AND METHODS

3.1. Chitosan Depolymerization

To depolymerize the commercial chitosan (Cognis), 500 ml of a solution of Chitosan 1% (w/v) in acetic acid (Panreac) 1% (v/v) was prepared. In order to obtain different chitosan molecular weights, different amounts of $NaNO_2$ (Sigma-Aldrich), shown in Table 3.1., dissolved in 10 ml of distilled water were mixed with chitosan and let this final solution under mechanic stirring for 1h at 1000 rpm. After 1h, a 4M NaOH (Merck) solution was added to the mixture until a pH of 9-10 was reached. The formed precipitate was centrifuge (Heraeus Multifuge X1R Centrifuge) for 10 min at 10000 rpm and washed with distilled water several times. Then, the precipitate was freeze dried for 24h (VaCo2 Zirbus Technology).

Table 3.1- Amount of $NaNO_2$ corresponding to the different CS/$NaNO_2$ ratio to obtain different chitosan molecular weight samples.

Ratio CS/$NaNO_2$	$NaNO_2$ (mg)
200-1	25
100-1	50
50-1	100
33-1	150
25-1	200

3.1.1. Chitosan Molecular Weight Determination

Capillary viscometry is a largely used technique to determinate polymers molecular weight. Figure 3.1A shows a viscosimetry apparatus where the time to determinate the sample viscosity is relatively short when compared with other techniques. Basically, it consists in comparing the time it takes a volume of diluted polymer solution to flow through a thin capillary with the time that a solvent takes to flow through the same capillary. It is a very simple measurement that consists in determinate the time that the solution takes to pass between two sensors, represented in Figure 3.1B by x and y, in a simple glass capillary. The only pressure difference between the top of the bulb and the bottom of the capillary is due to hydrostatic pressure, i.e. the weight of the liquid.

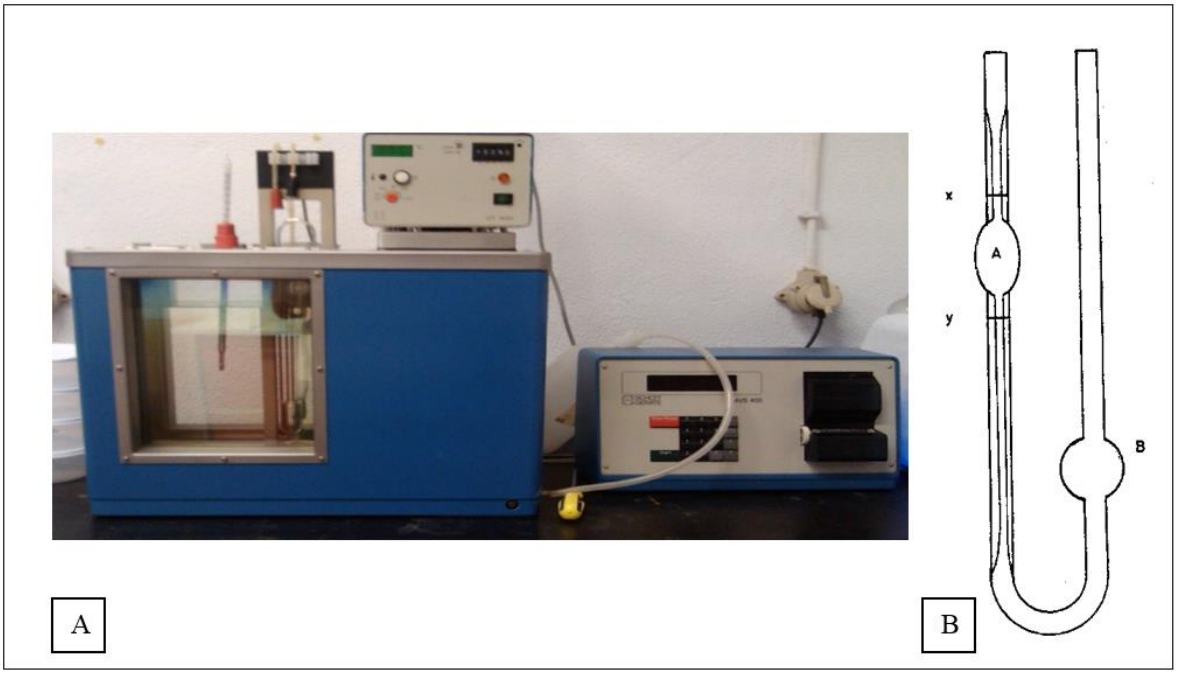

Figure 3.1 A, B- Viscosimetry apparatus used to determinate the chitosan molecular weight (A) and scheme of the capillary (B).

The polymer molecular weight is related to the intrinsic viscosity [η] by the Mark-Houwink-Sakurada (MHS) equation:

$$[\eta] = KM_v^a \quad \textbf{Eq. 2}$$

Where M_v is the viscosity-average molecular weight, and *K* and *a* are the constants for the solute-solvent system [59]. The values of MHS equation constants, *a* and *K*, were calculated using the following equations:

$$a = 0.6202 + \frac{0.699x}{(0.4806 + x)} \quad \textbf{Eq. 3}$$

$$logK.10^{-5} = -5.7676.a + 5.9232 \quad \textbf{Eq. 4}$$

Where x is [DA/pH. μ], with DA, chitosan degree of acetylation, pH of chitosan solution in a solvent with ionic strength of μ.[60]

This technique requires a solvent, 0.2M HAc/0.1M NaAc (Scharlau), to dilute the chitosan samples with different concentrations. Using equation **(3)** and **(4)**, the values of constants *a* and *K* were calculated to be 0.81 and 16.8 x 10^5 dL.g^{-1} [59]. For each sample the viscosity measurements were made in triplicate.

To determinate the chitosan molecular weight of the 5 samples produced by the depolymerization technique and the commercial chitosan itself viscometer (SCHOTT GERATTE AVS 400) was used.

3.2. Chitosan Nanoparticles Synthesis

Chitosan nanoparticles were prepared by ionic gelation technique using tripolyphosphate (TPP) (Sigma-Aldrich) [51]. For all the chitosan samples a 0.4% (w/v) chitosan solution with 1% (v/v) acetic acid was prepared and 0.25% (w/v) TPP solution of pH 5, 9, and 13.

To produce nanoparticles equal volumes of 0,25% (w/v) TPP and 0.4% (w/v) chitosan solutions were used, which were mixed during 5 minutes using *Turrax* (IKA T10 Basic).

3.3. Iron Oxide Nanoparticles Synthesis

Water-soluble Fe_3O_4 nanoparticles were prepared by thermal decomposition of $Fe(acac)_3$ (Alfa Aesar) in TREG (Sigma-Aldrich) at high temperature without using surfactant. Typically, 2 mmol of $Fe(acac)_3$ were dissolved in 20 ml of hydrophilic TREG media and then magnetically stirred (100 rpm) under a flow of nitrogen. The solution was dehydrated at 200ºC for 1h, and then quickly heated to 350 ºC and kept at this temperature for 2h.

The black solution was cooled to room temperature overnight by removing the heat source. The nanoparticles were precipitated by addition of 20 ml of ethyl acetate (Sigma-Aldrich) and then isolated by centrifugation (Heraeus Multifuge X1R Centrifuge) for 20 min at 10000 rpm.

This washing process was repeated and then the washed particles were dispersed in water to get a stable aqueous ferrofluid suspension [30].

3.3.1. Iron Content Determination

The iron concentration in the samples was determined using the 1,10-phenanthroline colorimetric method [61]. In detail, 40 µL of sample was transferred into a vial, followed by the addition of 20 µL of concentrated hydrochloric acid (37%, Fluka). The solution was incubated for 1h at room temperature to dissolve the SPIONs and to yield ferrous and ferric chloride. After, 100 µL of a hydroxylamine hydrochloride (Alfa Aesar) solution 100 mg/mL was added, to reduce Fe (III) to Fe (II), followed by the addition of 500 µL of 1,10 phenanthroline (Applichem) 3 mg/mL to form the orange-red complex of tris(1,10-phenanthroline) iron(II). Finally, the samples were diluted to 1800 µL using ammonium acetate (Panreac) 500 mM pH 4 buffer, which was also used in the reagents' solutions. The absorbance of the samples was measured at 510 nm using a UV-VIS spectrophotometer (T90+ UV/VIS Spectrometer PG Instruments Ltd). The concentration of iron (II) was calculated using a calibration curve using Mohr's salt solution in HCl 10 mM in a concentration range of 10 to 1000 µg/mL.

3.4. Chitosan Coated SPIONs

SPION nanoparticles suspensions were added to a 0.4% chitosan solution with 1% (v/v) acetic acid in a ratio of 0.5:1, 1:1, and 2:1 (v/v). To this solution was added 1 ml of TPP of pH 5, 9, and 13. Each sample was repeated 6 times, 3 of them were left in magnetic stirring for 24h at room temperature and the other 3 were left without stirring for 24h at room temperature.

3.5. Doxorubicin Encapsulation and Release

3.5.1. Doxorubicin Content Determination

The absorbance of the samples containing DOX was measured at 480 nm using a UV-VIS spectrophotometer (T90+ UV/VIS Spectrometer PG Instruments Ltd). The concentration of Doxorubicin was calculated using the following obtained calibration curve:

$$y = 0.0178x - 0.0011 \quad \textbf{Eq. 5}$$

Where y is the Doxorubicin concentration and x is the absorbance of the solution measured at 480 nm [62].

3.5.2. Evaluation of Doxorubicin Encapsulation

Different volumes of TPP 0.25% pH5 (500µl, 1000µl and 1500µl) were added to 500µl of 3:1 (w/w) CS-DOX solution using *Turrax* (IKA T10 Basic) and then centrifuged at 10000 rpm for 5min. Then the samples were washed with distilled water and centrifuged again at 10000 rpm for 5min. Supernatant DOX concentrations were calculated by UV-VIS spectroscopy (T90+ UV/VIS Spectrometer PG Instruments Ltd) with an emission wavelength at 480 mm. Dilutions of samples and calibration curves were performed in distilled water , and all measurements were performed in triplicate. Encapsulation Efficiency **(6)** and Drug Loading **(7)** were determined according to the following equations:

$$Encapsulation\ efficiency = \frac{total\ DOX - free\ DOX}{total\ DOX} \quad \textbf{Eq. 6}$$

$$Drug\ Loading(\%w/w) = \frac{Mass\ of\ drug\ loaded\ in\ NPs * 100}{Mass\ of\ nanoparticles} \quad \textbf{Eq. 7}$$

3.5.3. Evaluation of *in vitro* Doxorubicin Release

4500 µl of TPP 0.25% were added to 1500µl of 3:1 CS-DOX solution using *Turrax* for 5 minutes. The solution was centrifuged at 10000 rpm for 10min. Then the samples were washed with 3 ml of distilled water and centrifuged again at 10000 rpm for 5min. The pellet was ressuspended in 2 ml of

PBS 1x pH 7.4 or HAc 2M/NaAc 1M. One milliliter of nanoparticles suspension was placed inside a dialysis tube. The dialysis was performed against 10 ml of PBS 1x pH 7.4 or HAc 2M/NaAc 1M either at 25ºC or 37ºC.

To measure the Doxorubicin release, 3 ml of the release medium were taken from the dialysis apparatus, and replaced with fresh medium at pre-defined times. The amount of doxorubicin released was measured by UV-VIS spectroscopy against free DOX.

All measurements were performed in triplicate.

3.6. Characterization of Nanoparticles

Size and morphology of the nanoparticles were determined using transmission electron microscopy (TEM) and dynamic light scattering (DLS) while crystal structure was identified by X-ray diffraction (XRD). Surface charge and surface coating of the nanoparticles were analyzed by Fourier transform infrared spectroscopy (FTIR). Magnetic characterization of the nanoparticles was performed by SQUID magnetometry (S700X Cryogenic, Ltd.).

3.6.1. Transmission Electron Microscopy- TEM

The particle size and morphology of the nanoparticles were determined by transmission electron microscopy imaging (TEM, Hitachi H-8100 II) at *Instituto Superior Técnico* in Lisbon. This TEM offers 200 kV acceleration voltage with high brightness LaB6 thermionic electron source and phase contrast resolution of better than 0.27nm (point) and 0.14nm (line).

The samples were prepared by diluting the suspension with ultrapure water to a 1:100 ratio. Afterwards one drop of the solutions was evaporated on a carbon coated substrate. The specimen holder is equipped with two samples and was loaded to the observation chamber. Chitosan and iron oxide nanoparticles produced by thermal decomposition were investigated. The particle size distributions of the samples were obtained statistically by measuring the diameter of 100 nanoparticles using TEM images.

3.6.2. Dynamic Light Scattering- DLS

Chitosan nanoparticles and chitosan coated SPIONs hydrodynamic diameters were measured by means of dynamic light scattering (DLS) equipment (AvidNano) using the *bladecell*® at 20ºC. For each sample (with and without magnetic stirring and TPP with pH 5, 9 and 13), 5 µl of sample was used.

Each sample was done 6 times, 3 of them were left in magnetic stirring for 24h at room temperature and the other 3 were left without stirring for 24h at room temperature.

It was also studied the effect of *Turrax* on nanoparticles' diameter. In the preparation of the samples, it was used *Turrax* for 5 min to homogenize the samples.

3.6.3. Superconducting Quantum Interference Device- SQUID

Magnetic measurements were performed by 7T SQUID magnetometer (S700X Cryogenic, Ltd.) at *Instituto Superior Técnico* in Lisbon. The zero-field-cooled (ZFC) and field-cooled (FC) measurements were performed by cooling the sample to 5 K at zero fields or in the presence of an external field of 100 Oe, respectively. All the magnetic measurements were carried out within a temperature range 5-320 K. Isothermal magnetization curves were obtained for fields up to 5 T for temperatures of 10 and 320 K. Saturation magnetization (M_S) of chitosan coated magnetite particles were determined.

3.6.4. X-Ray Diffraction- XRD

The crystalline phases of the materials were verified using powder X-ray diffraction (XRD, PANAlyticalX'Pert PRO) using a Cu-Kα radiation (λ= 1.54060Å). Dry nanoparticles were obtained by freeze drying (Vaco2, Zirbus) a part of the suspension overnight. To obtain the XRD pattern of the particles 2θ values were taken form 15° to 80°, with a step size of 0.033. The Scherrer`s equation was used to measure the average crystallite size.

3.6.5. Fourier Transform Infrared Spectroscopy- FTIR

FTIR spectra of the samples were obtained using a Nicolet 6700 – Thermo Electron Corporation Total Reflectance-Fourier Transform Infrared spectrometer (ATR-FTIR). FTIR allows the detection of functional groups and the characterization of covalent bonding information. By this method, chemical changes of chitosan, iron oxide, chitosan coated magnetite nanoparticles, and chitosan coated magnetite nanoparticles loaded with doxorubicin were investigated.

3.6.6. Hyperthermia measurements

In a first step the hyperthermia capability of several concentrations of the uncoated NPs synthetize by Thermal Decomposition were tested for a frequency of 418.5 kHz, AC magnetic field intensity of 24 kA/m, 1 ml of the NPs sample and 40 minutes of field application. All the heating curves where adjusted to a mathematical model (Eq. 8) of the ZAR v1.0 software from Nb nanoscale Biomagnetics.

$$T(t) = \left(T_0 - T_{eq}\right)e^{-\frac{1}{\tau}t} + T_{eq} \quad \textbf{Eq. 8}$$

In the equation T_0 is the initial temperature of the sample, T_{eq} is the equilibrium temperature of the sample; T the maximum temperature reached by the sample and τ is characteristic time of heating.

3.7. Cell Line and Culture Conditions

3.7.1. Cytotoxicity Experiments

Day 1: unfreeze the cells

The first step to unfreeze the cells was to remove a sample with 1ml, around 2 million cells, from -80ºC and put them in a 37ºC water bath to accelerate the unfreeze process.

To a T25 bottle with 5ml of cellular solution (DMEM) with serum was added the previous unfreeze sample with 1ml of cells. This solution was allowed in an incubator with constant temperature (37ºC). Some hours later, the cellular solution was replace in order to remove the toxic DMSO (unfreeze agent).

Day 2: Cell seeding

The solution of the previously unfreeze cells was removed and washed with PBS 1x solution (5ml) without Ca and Mg. Then, the PBS solution was removed and 500 µl of tripsin was added at 37ºC in the incubator for 5 minutes. The sample was gently agitated and a 5ml mixture of DMEM solution and Glutomax 1x (Gibco) was added. For each well it was pipetted 100 µl of the previously solution (cells were counted before) and was left in incubator at 37ºC for 24 hours.

Day 3: Add the NPs synthetized into the NPs cells

The last step was to add the lyophilized and sonicated chitosan, magnetite and chitosan coated iron oxide nanoparticles into the cells previously seed. For each well, the DMEM solution was removed and NPs solution was added. To the first line of wells, a 5 mg/ml NPs solution in DMEM was added and then a 1:2 dilution was performed to have different concentrations of NPs. For each concentration it was made 4 replicas. The plate with the mixture of cells and NPs was left in the stove at 37ºC for 24 hours.

Day 4: Cellular Viability determination

In order to determinate the cellular viability it was necessary to prepare the samples to measure the absorbance in UV-Vis equipment at 570 and 600 nm. Each well was washed several times with PBS.

After that, 100 µl of resazurine and cellular solution was added to each well and left in the stove for 2 hours.

4. RESULTS AND DISCUSSION

4.1. Chitosan Characterization

The main goal of the present work was to produce chitosan nanoparticles that could be used in drug delivery systems. Before the production of these nanoparticles it was necessary to obtain and characterize different molecular weight samples of commercial chitosan. In the present section 4.1 is described the results obtained for the different chitosan molecular weight samples and their characterization.

4.1.1. Chitosan Molecular Weight Determination

Viscosimetry measurements used to determinate the chitosan molecular weight (CS M_v) are shown in this section. The main goal of this procedure was to decrease the CS M_v in order to study the influence of M_v in the CS NPs' diameters and their properties. In order to decrease the molecular weight of chitosan was used different amounts of an oxidant agent - $NaNO_2$ - keeping all others conditions unchanged.

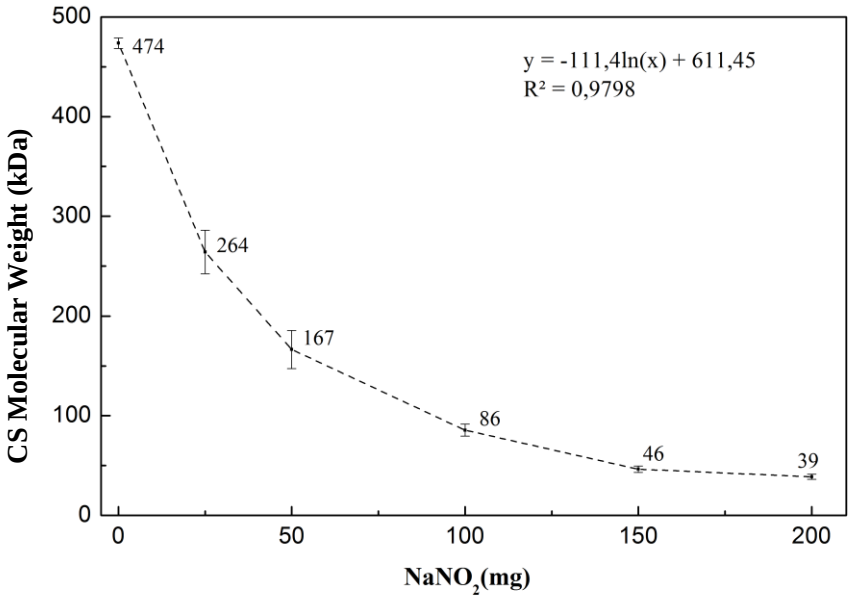

Figure 4.1- Chitosan molecular weight values calculated by viscosimetry using different amounts of $NaNO_2$.

As can be seen in Figure 4.1, the commercial CS M_v was 474 kDa, determined without addiction of $NaNO_2$. Different CS samples with M_v between 264 - 39 kDa by the depolymerization technique were obtained, using different amounts of $NaNO_2$ (25-200 mg).

Table 4.1- Chitosan molecular weight values and their standard deviation and depolymerization efficiency.

$NaNO_2$ (mg)	CS (g)	MW (kDa)	S.D	Efficiency (%)
0	5	474	5	
25		264	22	99.0
50		167	19	99.6
100		86	6	98.0
150		46	3	85.4
200		39	2	92.6

Table 4.1 shows chitosan molecular weight values obtained through depolymerization of 474 kDa commercial chitosan. As seen before the depolymerization was obtained by an oxidation reaction of the commercial chitosan using $NaNO_2$ as an oxidant agent. Figure 4.1 and table 4.1 show the decrease of the chitosan molecular weight with increase of $NaNO_2$. The degree of efficiency for the 5 depolymerizations is quite high, representing an efficiency above 85% for all chitosan's molecular weights.

It can be concluded, from the results shown in Figure 4.1 and Table 4.1, that the depolymerization technique is an efficient procedure to decrease the CS molecular weight.

4.1.2 Chitosan chemical Characterization

FTIR measurements were performed in order to examine the chemical structure of chitosan for different degrees of depolymerization. In Figure 4.2 FTIR spectra are presented for the four molecular weights of chitosan obtained by the depolymerization of commercial chitosan. Some characteristic bands, arising from the presence of amine and methylene groups on chitosan, are observed. Bands at 2924 cm^{-1} and 2852 cm^{-1} are assigned to the CH_2 antisymmetric and symmetric stretching modes, respectively. Due to the presence of amine group, a band at ~1600 cm^{-1} is assigned to the bending mode of N-H and other at ~ 1080-1360 cm^{-1} is assigned to C-N stretching modes.

For all molecular weights of chitosan analysed on this study, FTIR spectra exhibits the same characteristic absorption bands due to the presence of methylene and amine groups on chitosan structure. However, the intensity of N-H band increases with decreasing CS M_v which means that the CS degree of deacetylation changes but with no significant impact in equations (2) and (3) for CS MW determination. Summing up, the FTIR analysis shows that the depolymerization of chitosan does not change its chemical structure.

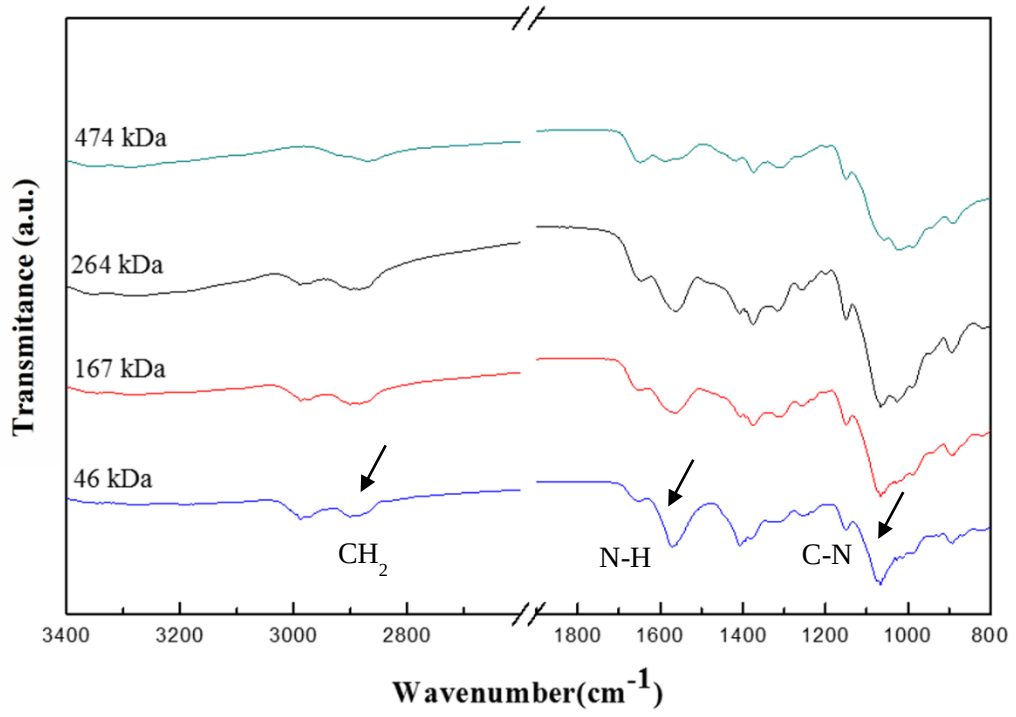

Figure 4.2- FTIR spectra for different chitosan molecular weight between 3400 and 800 cm^{-1}.

4.2. Chitosan Nanoparticles Characterization

After the characterization of the different molecular weight chitosan samples the next goal of the present work was to produce chitosan nanoparticles by ionic gelation technique. To produce them it was necessary to study the influence of some parameters in the chitosan nanoparticles diameter, such as chitosan molecular weight, pH, magnetic stirring and the use of *Turrax* equipment. The characterization of chitosan nanoparticles is also described in section 4.2 as well as the results obtained by the study of the mentioned parameters.

4.2.1. Chitosan Nanoparticles Diameter

DLS measurements were made in order to analyze chitosan nanoparticles diameters. For each chitosan molecular weight obtained in the previous section 4.1, the CS NPS diameter was analyzed under different conditions of pH (pH5, 9 and 13) and agitation (with and without magnetic stirring (Agt.)). The results of this study are shown in Figure 4.3 and Table 4.2.

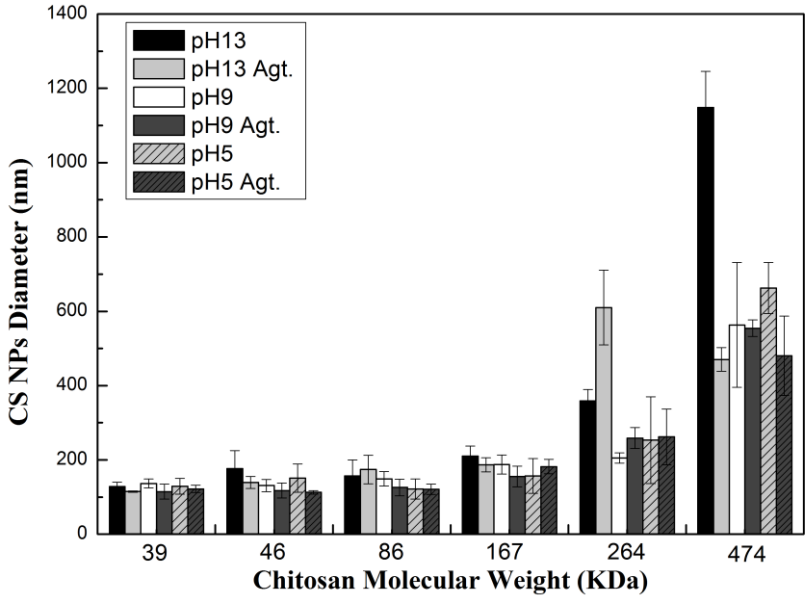

Figure 4.3- Chitosan nanoparticles diameter (nm) for different molecular weight, pH and magnetic stirring (Agt.).

The samples with lower molecular weight, 39 – 167 kDa and considering the standard deviation, exhibit a diameter below 200 nm for the different pH and agitation used and mentioned above. This behavior is not observed for the 264 and 474 kDa samples. Chitosan nanoparticles produced using these chitosan molecular weights present higher diameters, particularly for pH 13 with and without agitation for 264 and 474 kDa respectively.

Figure 4.3 shows that the chitosan nanoparticles diameters increaese with increasing chitosan molecular weight. Although there are not significant differences between pH 5, 9, and 13 with the exception of pH 13 in the higher chitosan molecular weight (264 and 474 kDa). The magnetic stirring does not display a homogeneous result for all CS Mw. In some cases the particles are smaller with magnetic stirring (39 and 46 kDa for pH 5, 9 and 13) whereas on other Mw it does not show any influence.

The parameters, pH and agitation, that result in smaller diameters for each chitosan molecular weight nanoparticles are resumed and shown in Table 4.2.

Table 4.2- Chitosan molecular weight parameters to obtain smaller chitosan nanoparticles diameters

CS (kDa)	474	264	167	86	46	39
pH	13	9	9	5	5	9
Magnetic stirring	✓	✗	✓	✓	✓	✓
Diameter (nm)	470 ± 31	205 ± 14	157 ± 47	121 ± 14	113 ± 5	115 ± 20

As can be seen in Figure 4.3 and Table 4.2 the influence of magnetic stirring is not very strong. To complement this study another procedure and equipment was used to prepare chitosan nanoparticles and to measure its diameters – *Turrax* (IKA T10 Basic).

It was used a sample of 46 kDa chitosan pH 5 (one of the parameters conjugation to obtain smaller diameters, as shown in Table 4.2) to study the influence of *Turrax* in the chitosan nanoparticles diameter and to be possible to compare the magnetic stirring with *Turrax*.

Table 4.3- Chitosan nanoparticles diameter and standard deviation for different *Turrax* time periods

Time (min)	Diameter (nm)	S.D.
5	115	9
10	150	10
15	154	8
20	138	14

It was performed a time study in order to understand for how long the *Turrax* needs to be used to obtain the smaller diameter in CS NPS. Time periods between 5 to 20 min were used. For the lower period, 5 min, a diameter around 115 nm was obtained and for the higher period, 20 min, a diameter around 138 was obtained. From Table 4.3 it can be seen that the lower diameter is obtained when *Turrax* is used for only 5 minutes.

Taking into account the previous time study, chitosan nanoparticles diameters were studied using *Turrax* for 5 min for each chitosan molecular weight. Diameters values obtained are shown in Figure 4.4.

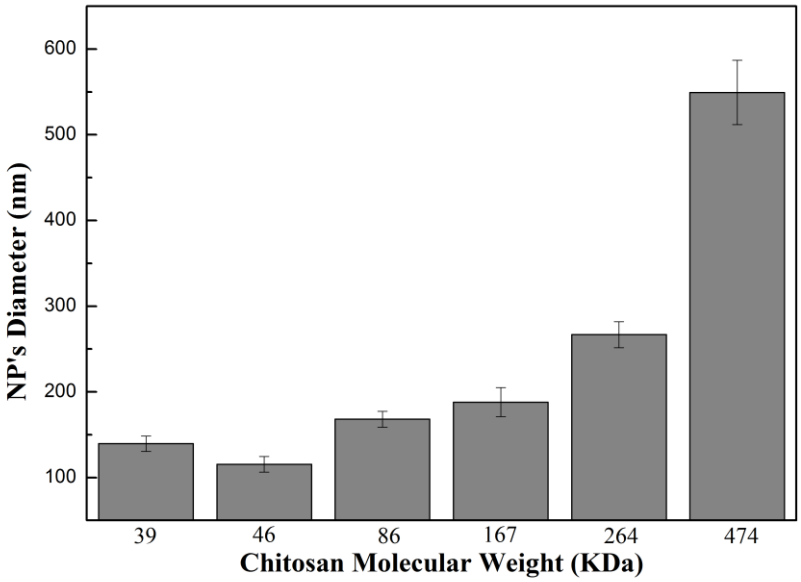

Figure 4.4- Chitosan nanoparticles diameter (nm) for different molecular weight using *Turrax* equipment.

The samples with chitosan molecular weight between 39 and 167 kDa exhibit a diameter below 200 nm. This value is not the same for the higher chitosan molecular weight samples. Chitosan nanoparticles produced using these chitosan molecular weights present higher diameters, around 300 and 550 nm for 264 and 474 kDa respectively.

Figure 4.4 shows that chitosan nanoparticles diameters increase with increasing chitosan molecular weight as it was seen in Figure 4.3. Note that although the diameters are similar to those obtained previously, the standard deviation is much smaller compared to the ones shown in Figure 4.3. Another relevant aspect is that the *Turrax* is faster than magnetic stirring. Therefore nanoparticles with the same diameter can be obtained with only 5 minutes instead of 24 hours of agitation.

4.2.2. CS NPs chemical characterization

In order to examine the chemical structure of chitosan nanoparticles produced in the previous section FTIR measurements were performed. FTIR spectra, between 4000 and 600 cm^{-1}, are presented in Figure 4.5 for commercial chitosan nanoparticles (a) obtained by ionic gelation technique as well as TPP (b) and chitosan (c) separately.

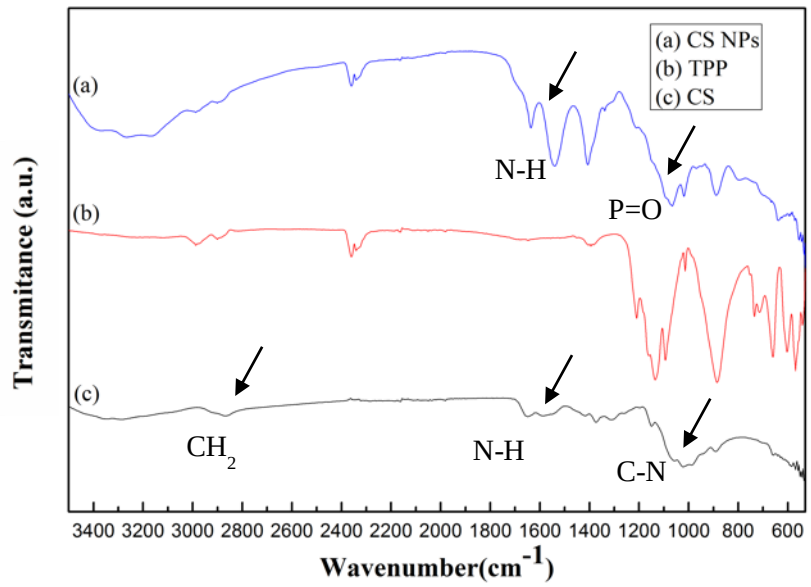

Figure 4.5- FTIR spectra for chitosan nanoparticles, TPP and chitosan between 3400 and 600 cm^{-1}.

Some characteristic bands, arising from the presence of amine and methylene groups on chitosan, are observed. Bands at 2924 cm^{-1} and 2852 cm^{-1} are assigned to the CH_2 antisymmetric and symmetric stretching modes, respectively. Due to the presence of amine group, a band at ~1600 cm^{-1} is assigned to the bending mode of N-H and other at ~ 1080-1360 cm^{-1} is assigned to C-N stretching modes [63].

In chitosan nanoparticles the band at 3438 cm^{-1} has a shift to 3320 cm^{-1} and becomes wider with increased relative intensity indicating an enhancement of hydrogen bonding. In nanoparticles the peaks for N-H bending vibration of amine I at 1600 cm^{-1} and the amide II carbonyl stretch at 1650 cm^{-1} shifted to 1540 cm^{-1} and 1630 cm^{-1}, respectively. The cross-linked chitosan also show a P=O peak at 1170 cm^{-1}. These results have been attributed to the linkage between phosphoric and ammonium ion. So we conclude that the tripolyphosphoric groups of TPP are linked with ammonium groups of chitosan. The inter- and intra-molecular actions are enhanced in chitosan nanoparticles [63].

4.3. Iron Oxide Nanoparticles Characterization

Considering that the chitosan nanoparticles have been produced and characterized as stated in the previous sections, another important goal of the present study includes the production of iron oxide nanoparticles by thermal decomposition technique as well as the study of their diameter and magnetic properties.

Several techniques were used to characterize the iron oxide nanoparticles synthesized. One of those techniques was phase identification (Structural characterization) performed by X-ray diffraction (XRD).

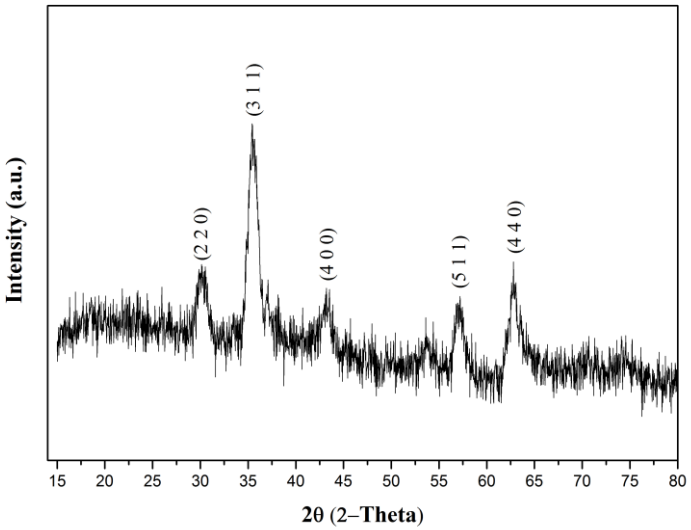

Figure 4.6- XDR spectrum with the characteristic peaks of iron nanoparticles.

It can be clearly identified, from Figure 4.6, the characteristic diffraction peaks of crystalline cubic magnetite structure in particular to 2θ = 30.12, 35.43, 43.22, 57.19 and 62.80 [64]. Narrower peaks represent the samples' crystalline structure. The XRD pattern of this sample was assigned to the phase of bulk magnetite.

The average crystallite size, τ , was calculated to be 13.54 nm using the Scherrer's equation $\tau = \frac{K\lambda}{\beta cos\theta}$, where K is the grain shape factor (K = 0.94); λ is the incident X-ray wavelength (λ = 0.15406 nm); β denotes the full width at half-maximum (in radians) of the highest intensity peak (β= 0.02532 rad), and θ is the corresponding diffraction angle (2θ = 35.43 ⇔ θ=17.715) corresponding to (311).

Size, shape and particle size distribution of the iron oxide nanoparticles were determined by TEM image analysis represented in Figure 4.7.

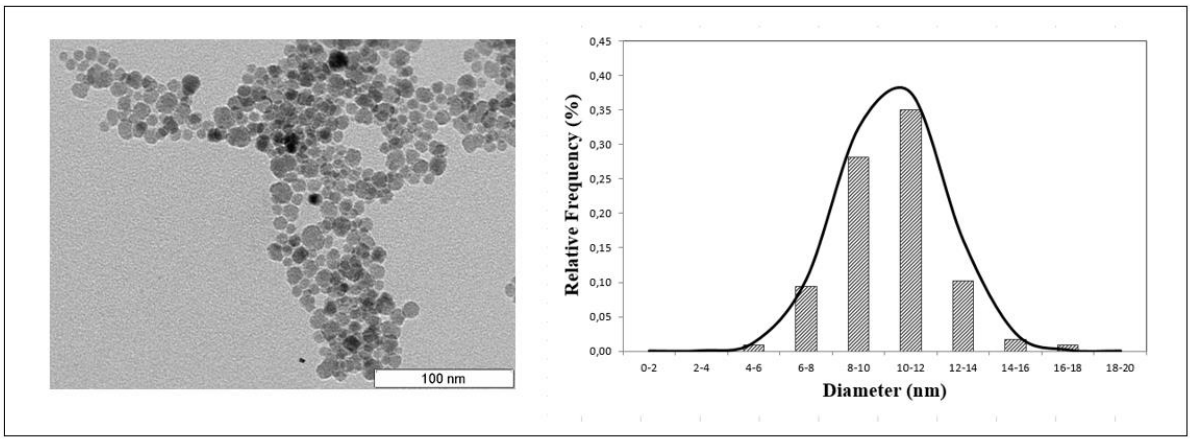

Figure 4.7- Iron Oxide nanoparticles TEM image and respective particle size distribution.

Figure 4.7 shows iron oxide nanoparticles dispersed in water. These nanoparticles present a roughly spherical morphology and were not bonded. The particle size was determined by statistical analysis of the dimensions of at least 100 particles yielding an average particle diameter of 10.3 ± 2.0 nm. This value agree with the value obtained from XRD data τ = 13.54 nm. The small difference observed in the particles diameter could be due to reduced accuracy of XRD technique comparatively to TEM. Reduced accuracy are related to high surface area that originates defects in the particles surface, high interfacial tension between particles that correspond to an expansion of diffraction and due to the fact that nanoparticles could be crystalline, amorphous or quasi crystalline [65].

4.3.1. Magnetic Properties

To characterize the magnetic properties of Fe_3O_4 nanoparticles, hyperthermia and SQUID measurements were performed.

Hyperthermia studies were performed in order to evaluate the ability of iron oxide nanoparticles on generating heat. Several concentrations of iron were tested as shown in Figure 4.8.

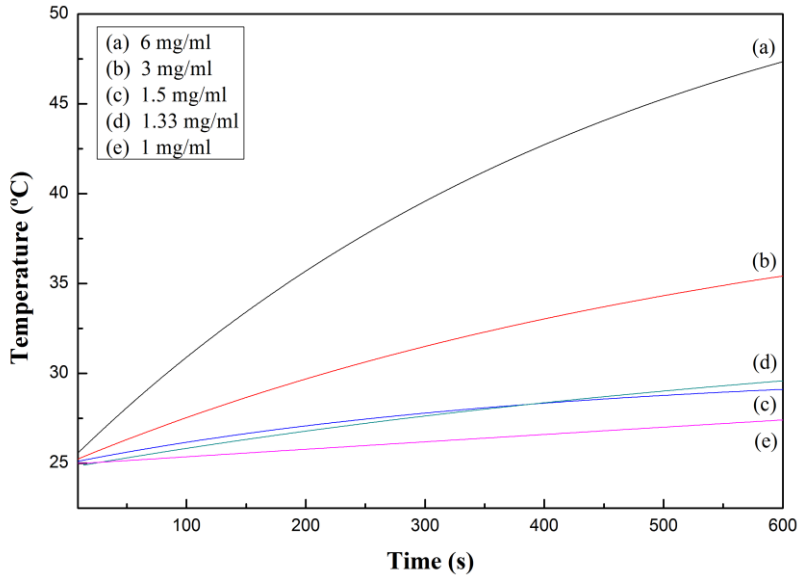

Figure 4.8- Hyperthermia curves of Fe_3O_4 nanoparticles synthetized by thermal decomposition with different iron concentrations.

Figure 4.8 show that concentrations below 1.5 mg/ml (c) possess a smaller ability to generate heat once the temperature only increases less than 5 ºC. On the other hand, concentrations above 1.5 mg/ml

present higher generated heat ability, as can be seen in the sample of 3mg/ml (b) and 6 mg/ml (a). The 6 mg/ml sample presents a temperature increase around 22.5ºC.

In summary, Fe_3O_4 nanoparticles synthesized by Thermal Decomposition technique possess the ability to generate heat. It can be seen that the heating ability of these nanoparticles rises with increasing of iron concentration.

Specific Absorption Ratio (SAR) is used to characterize the heating efficiency that a magnetic material possess by measuring the energy absorption when that material is expose to an alternative magnetic field. It is defined as the power absorbed per mass unit and it units are watts per gram (W/g). SAR is calculated by the following equation:

$$SAR\left(^{W}/_{g}\right) = \left(\frac{\partial T}{\partial t}\right)_{max} x \frac{C_{NP}\ x\ m_{Fe}\ x\ C_l m_l}{m_{Fe}} \qquad \textbf{Eq. 9}$$

where $\left(\frac{\partial T}{\partial t}\right)_{max}$ is the maximum gradient of the temperature curve of the colloid submitted to a hyperthermia test, C_{NP} is the specific heat of the nanoparticles, C_l is the specific heat of the liquid, m_l is the fluid mass, and m_{Fe} is the iron mass in the colloid [66].

SAR values of the same colloid measured under different experimental conditions (external magnetic field intensity - *H* - and frequency - *f* - of the applied magnetic field) will be different, making impossible to directly compare results obtained in different laboratories or equipment. For this reason intrinsic loss Power (ILP) has been proposed because it is independence of the field used and the equipment [66]. It is defined as:

$$ILP\left(\frac{\mathrm{nH}m^2}{\mathrm{Kg}}\right) = \frac{SAR}{fH^2} \qquad \textbf{Eq. 10}$$

Table 4.4- SAR and ILD values for each Iron concentration of Fe_3O_4 nanoparticles synthetized by Thermal Decomposition.

[Fe] (mg/ml)	**SAR** (w/g)	**ILP** (nH.m^2/kg)
6	**51.1**	0.214
3	**43.9**	0.143
1.5	**37.9**	0.159
1.33	**34.6**	0.145
1	**28.9**	0.121

Table 4.4 shows the SAR values obtained by the maximum of $\left(\frac{\partial T}{\partial t}\right)$ which occurs in the beginning of the hyperthermia measurements, when adiabatic conditions were guaranteed. It can be seen that SAR and iron concentration values are proportional. This means that higher iron concentrations correspond to higher heating efficiencies of the Fe_3O_4 nanoparticles. The same occurs to ILP values, iron concentrations values are proportional to ILP values and that correspond to higher heating efficiencies of the Fe_3O_4 nanoparticles.

In order to evaluate the superparamagnetic properties of Fe_3O_4 nanoparticles produced, SQUID measurements were performed. The results obtained with this study are shown in Figure 4.9.

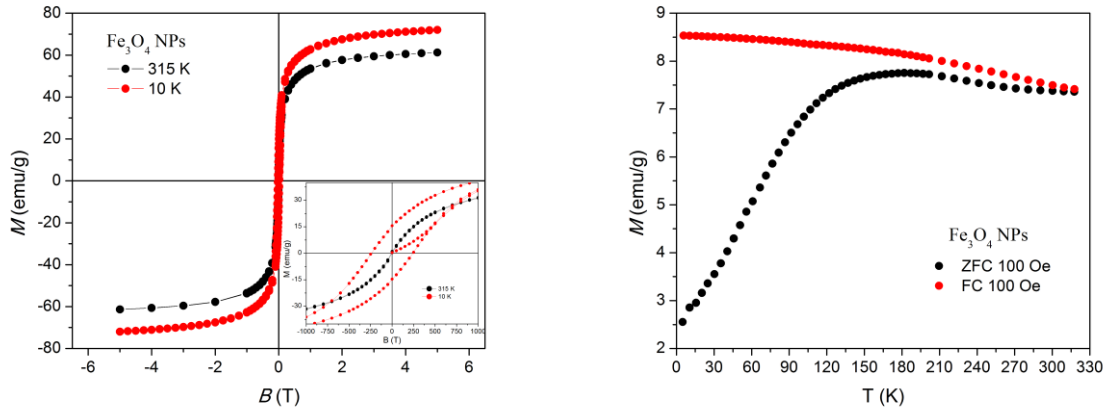

Figure 4.9- Left: magnification of the hysteresis loops of Fe_3O_4 measured at 10 K and 315 K. The below right inset correspond to the magnification of hysteresis loops at the same temperatures with a different magnetic field scale. Right: temperature dependence of the zero-field cooled/field cooled (ZFC-FC) magnetization of the magnetite nanoparticles measured by SQUID under an applied field of 100 Oe.

Figure 4.9-Left shows a magnification of the hysteresis loops of Fe_3O_4 measured at 10 K and 315 K. The below right inset correspond to the magnification of hysteresis loops at the same temperatures with a different magnetic field scale. It is evident the absence of coercivity and remanence at 315 K. This indicates the superparamagnetic behavior of Fe_3O_4 nanoparticles at this temperature.

Superparamagnetism is a form of magnetism, which appears in small nanoparticles (< 30 nm). In the absence of an external magnetic field, their magnetization appears to be in average zero: they are said to be in the superparamagnetic state. In this state, an external magnetic field is able to magnetize the nanoparticles, similarly to a paramagnet. However, their magnetic susceptibility is much larger than that of paramagnets.

Figure 4.9-Right shows the temperature dependence of the zero-field cooled/field cooled (ZFC-FC) magnetization of the magnetite nanoparticles measured by SQUID under an applied field of 100 Oe. The maximum of ZFC curve is reached about 165 K which means that above that temperature, called blocking temperature (T_B), the sample is superparamagnetic and below is ferromagnetic. At room temperature (315 K) the sample is superparamagnetic.

4.4. Chitosan coated Iron Oxide Nanoparticles

On previous sections it was described the chitosan and Fe_3O_4 nanoparticles synthesis by ionic gelation and thermal decomposition respectively and its characterization by a battery of techniques.

The next step, that was the main goal of the present study, was to join the two synthesized nanoparticles in order to form the chitosan coated iron oxide nanoparticles. In the present section is described all characterization techniques that were used to characterize them.

4.4.1. Chitosan coated Iron Oxide Nanoparticles Diameter

One of the characterization techniques used was DLS measurements to obtained chitosan coated iron oxide nanoparticles diameter.

In Figure 4.10 it can be seen the diameter values obtained for all the parameters studied. For each chitosan molecular weight was studied the influence of pH (5, 9, and 13), agitation (with and without agitation) as well as different CS/SPIONS ratios (0.5-1; 1-1; 2-1).

The set of parameters that result in the smaller diameter is not the same for each chitosan molecular weight. For the 39 kDa chitosan samples, pH 13 with agitation and CS/SPIONs ratio 2-1 are the best set of parameters to obtain the smaller diameter - 146±3 nm. For 46 kDa chitosan the parameters are the same with the exception of agitation, in this case without it, that result in diameters around 68±4 nm. The samples related to 86 kDa chitosan exhibit a diameter around 144±6 nm that results from pH 13 with agitation and CS/SPIONs ratio 1-1. Samples using 167 kDa chitosan present a 213±34 nm diameter that results from pH 9 with agitation and CS/SPIONs ratio 0.5-1. The samples with 264 kDa chitosan show a 210±5 nm diameter that was obtained from pH 5 with agitation and CS/SPIONs ratio 2-1. The commercial chitosan (474 kDa) present a 232±1 nm diameter resultant from pH 13 with agitation and CS/SPIONs ratio 1-1.

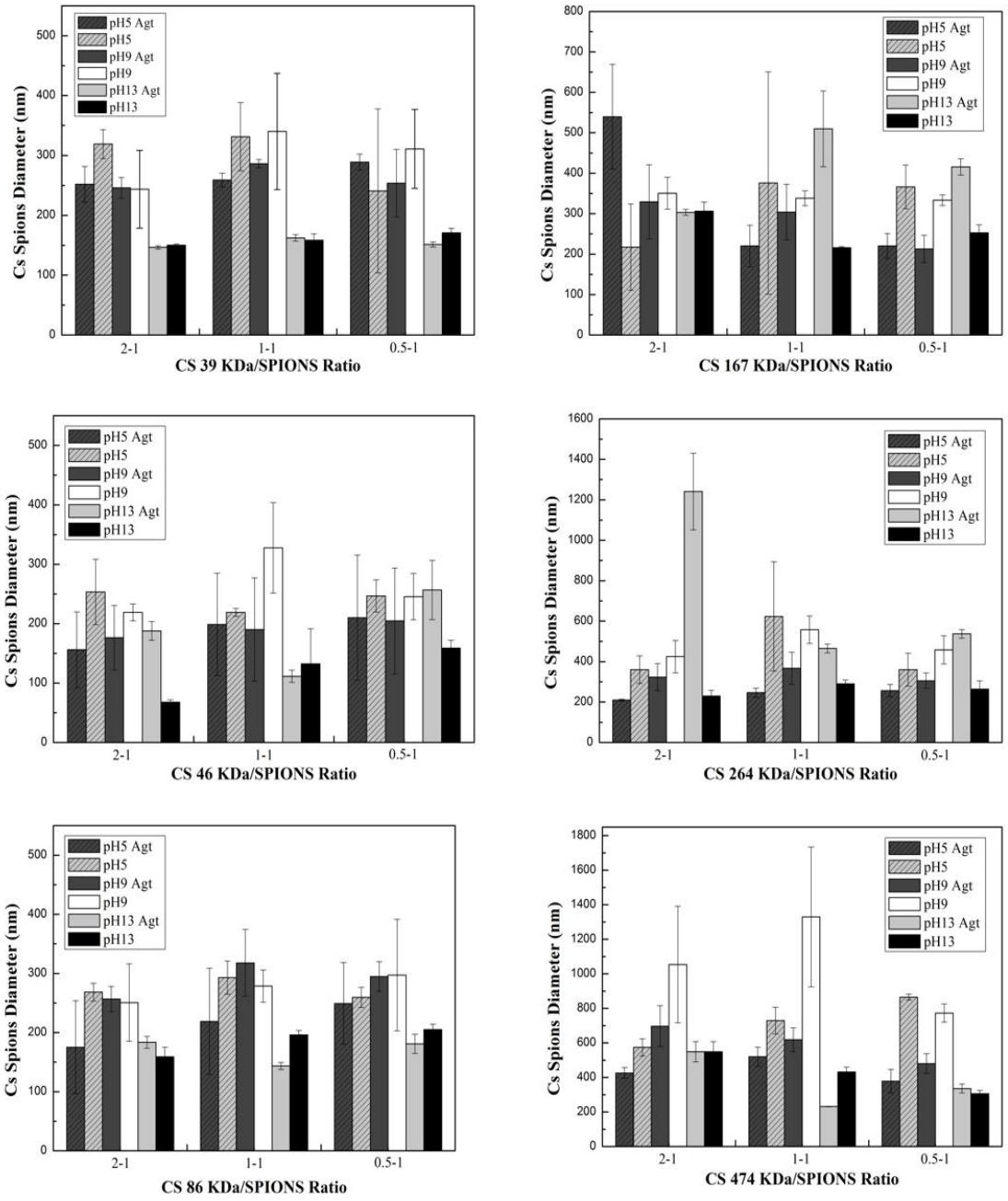

Figure 4.10- Chitosan coated iron oxide nanoparticles (CS SPIONs) diameters. Each chitosan molecular weight is represent in one graph where is represented the influence of pH 5, 9, and 13 with and without agitation (Agt.) as well as different CS/SPIONS ratios (0.5-1; 1-1; 2-1).

All the analysis made above is resumed in Table 4.5 which contains the best parameters conjugation that correspond to the smaller chitosan coated iron oxide nanoparticles diameters.

Table 4.5 - Chitosan molecular weight, pH, agitation, and Cs/SPIONs Ratio parameters to obtain smaller chitosan coated iron oxide nanoparticles diameters

S (kDa)	474	264	167	86	46	39
pH	13	5	9	13	13	13
Agitation	✓	✓	✓	✓	✗	✓
Cs/SPIONs Ratio	1-1	2-1	0,5-1	1-1	2-1	2-1
Diameter(nm)	232±1	210±5	213±34	144±6	68±4	146±3

Considering Figure 4.10 and Table 4.5 analysis, pH 13 seems to be the best pH to be used and magnetic stirring gives smaller diameters. On the other hand, CS/SPIONs ratio depends on which chitosan molecular weight is being used. The smaller diameter - 68±4 - was obtained with CS 46 kDa, pH13 without magnetic stirring and CS/SPIONs ratio 2-1. Should be noted that the standard deviation are relatively large in some samples which must be taking into account in the analysis made in this section.

4.4.2. CS coated SPIONs Chemical Characterization

In order to examine the structure of chitosan coated iron oxide nanoparticles produced, FTIR measurements were performed between 4000 and 600 cm^{-1}. FTIR spectra are presented in Figure 4.11 for commercial chitosan coated iron oxide nanoparticles (a), 39 kDa chitosan coated iron oxide nanoparticles (b) as well as commercial chitosan (c) and iron oxide (d) separately.

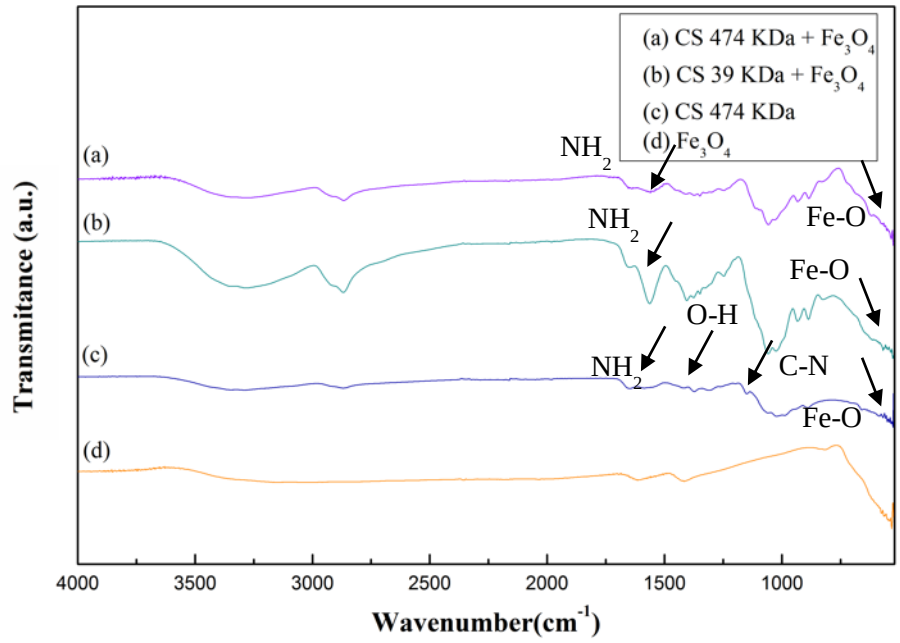

Figure 4.11- FTIR spectra for chitosan 474 kDa coated iron oxide nanoparticles (a); chitosan 39 kDa coated iron oxide nanoparticles (b); chitosan 474 kDa (c) and Iron oxide (d) between 4000 and 600 cm^{-1}

To confirm the chemical composition of synthesized nanoparticles, FTIR spectra were obtained. The presence of Fe_3O_4 core could be identified by the strong stretching absorption band at 579 cm^{-1}, which corresponded to the Fe–O bond. The band located in the 583 cm^{-1} region is found in bare and chitosan-coated nanoparticle's spectra, confirming that the products contain magnetite. The bands around 1615±15 cm^{-1}, assigned to the NH_2 group bend scissoring, are present in both chitosan and chitosan-coated nanoparticle's spectra, proving that magnetite nanoparticles were successfully coated by chitosan polymer. In the IR spectrum of chitosan the band at 1628 cm^{-1} is assigned to NH_2 group bend scissoring, the band at 1422 cm^{-1} to OH bending of primary alcoholic group, and 1156 cm^{-1} to C–N stretch in chitosan. In the spectrum of chitosan coated iron oxide nanoparticles, the 1628 cm^{-1} band of NH_2 group bend scissoring in chitosan, shifted to 1618 cm^{-1} and a new sharp band at 583 cm^{-1} has appeared. All characteristic bands of chitosan and iron oxide were present in the spectrum of chitosan coated iron oxide nanoparticles. Results indicated that iron oxide nanoparticles were successfully coated with chitosan and these results are compatible with results in the literature [67].

4.4.3. Magnetic Properties

To characterize the magnetic properties of chitosan coated Fe_3O_4 nanoparticles, as it was done for the Fe_3O_4 nanoparticles, hyperthermia and SQUID measurements were performed.

Hyperthermia studies were performed in order to evaluate the ability that the chitosan coated iron oxide nanoparticles possess to generate heat. Several CS/TPP ratios were tested for 39 kDa and 474 kDa chitosan as can be observed in Figure 4.12.

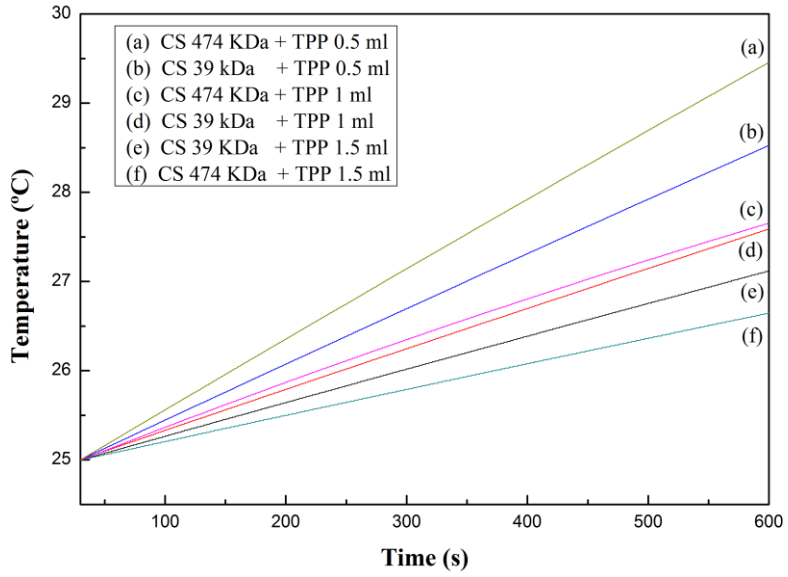

Figure 4.12- Hyperthermia curves of chitosan coated Fe_3O_4 nanoparticles with different chitosan molecular weights (39 and 474 kDa) and TPP volumes (0.5, 1 and 1.5 ml).

Figure 4.12 shows that nanoparticles synthetized using 0.5 ml of TPP for both 474 kDa (a) and 39 kDa (b) chitosan present higher generated heat ability once the temperature increases around 4 ºC. On the other hand, nanoparticles synthetized using 1 ml of TPP for both 474 kDa (c) and 39 kDa (d) chitosan possess a smaller ability to generate heat once the temperature only rises less than 2.5 ºC. At last, nanoparticles using 1.5 ml of TPP, (e) and (f), exhibit a temperature increase of less than 2 ºC which indicates a lower ability to generate heat.

Chitosan coated Fe_3O_4 nanoparticles synthesized possess the ability to generate heat as shown in Figure 4.12. It can be seen that the heating ability of this nanoparticles rises with decreasing TPP volumes. In fact, when the volume of TPP is increased chitosan crosslinking increases which leads to a decrease in the heat generating ability of this nanoparticles.

It can be concluded that the TPP volume has more influence in the heating ability than the chitosan molecular weight. However, for the same TPP volume, for the 3 volumes studied, CS 474 kDa possesses a higher heating ability than CS 39 kDa.

SAR and ILP values were calculated and are resumed in Table 4.6 considering the same chitosan coated iron oxide nanoparticles used in Hyperthermia measurements.

Table 4.6- SAR and ILD values for chitosan coated iron oxide nanoparticles synthetized with different iron concentrations, CS MW and TPP volumes.

Sample	[Fe] mg/ml	SAR [w/g]	ILP [nH.m^2/kg]
CS 39 kDa + TPP 0.5 ml	2	12.6	0.053
CS 39 kDa + TPP 1 ml	1.33	10.1	0.042
CS 39 kDa + TPP 1.5 ml	1	7.9	0.033
CS 474 kDa + TPP 0.5 ml	2	20.5	0.086
CS 474 kDa + TPP 1 ml	1.33	17.6	0.074
CS 474 kDa + TPP 1.5 ml	1	8.8	0.037

For each chitosan molecular weight, 39 kDa and 474 kDa, were used 3 TPP volumes which correspond to 3 different iron concentrations.

Table 4.6 shows that SAR and TPP volumes are inversely proportional. However, increasing volumes of TPP correspond to a decrease of the iron concentration present on the nanoparticles. This means that higher iron concentrations correspond to higher heating efficiencies of the chitosan coated Fe_3O_4 nanoparticles as well as it was seen for Fe_3O_4 nanoparticles. The same analysis can be made to ILP values obtained, higher iron concentrations correspond to higher heating efficiencies.

As observed before in Figure 4.12, SAR and ILP values obtained corroborate the idea that CS 474 kDa possesses a higher heating ability than CS 39 kDa nanoparticles since SAR and ILP values are higher when 474 kDa chitosan was used.

In the same way for Fe_3O_4 nanoparticles, SQUID measurements were performed to evaluate the superparamagnetic properties of chitosan coated Fe_3O_4 nanoparticles.

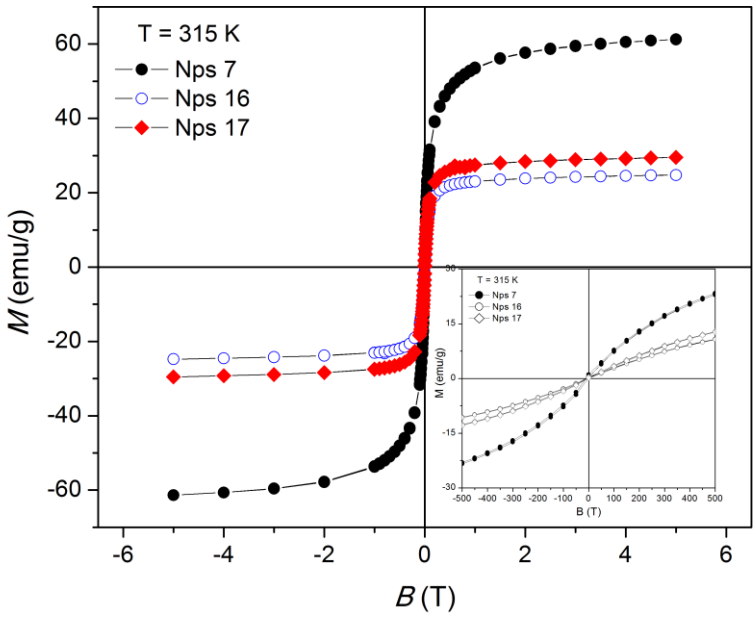

Figure 4.13- Magnification of the hysteresis loops of chitosan coated Fe_3O_4 measured at 315 K. The below right inset correspond to the magnification of hysteresis loops at the same temperatures with a different magnetic field scale.

Figure 4.13 shows a magnification of the hysteresis loops of Fe_3O_4 nanoparticles (Nps7) and chitosan coated Fe_3O_4 nanoparticles using 39 kDa (NPs 16) and 474 kDa (NPs 17) chitosan measured at 315 K. The below right inset correspond to the magnification of hysteresis loops at the same temperature with a different magnetic field scale. It can be observed the absence of coercivity and remanence at 315 K. This indicates the superparamagnetic behavior of chitosan coated Fe_3O_4 nanoparticles using 39 kDa and 474 kDa chitosan at this temperature.

4.5. Doxorubicin Encapsulation and Release

Considering that chitosan nanoparticles was already synthetized and characterized, in the present section it is present the results for Doxorubicin encapsulation and release. To study the encapsulation, it was used the higher and lowest chitosan molecular weight (474 and 39 kDa). On the other hand, to

study the release more samples of chitosan (474, 264, 167 and 39 kDa) were used to understand the influence of molecular weight in drug release.

4.5.1. Evaluation of Doxorubicin Encapsulation

In order to study the encapsulation of Doxorubicin in the chitosan nanoparticles, the Encapsulation Efficiency – EE (%) – and Drug Loading (%w/w) were determined using the following equations:

$$Encapsulation\ efficiency = \frac{total\ DOX - free\ DOX}{total\ DOX} \quad \textbf{Eq. 11}$$

$$Drug\ Loading(\%w/w) = \frac{Mass\ of\ drug\ loaded\ in\ NPs * 100}{Mass\ of\ nanoparticles} \quad \textbf{Eq. 12}$$

The values needed to calculate EE (%) and DL (%w/w) presented in Table 4.7, were obtained using UV-VIS spectrophotometer. The mass of nanoparticles were estimated by adding the mass of chitosan and TPP used in each sample.

Table 4.7- Encapsulation Efficiency (EE) and Drug Loading (DL) values for Doxorubicin encapsulation on chitosan nanoparticles with 39 and 474 kDa and different volumes of TPP.

Cs MW (kDa)	TPP (µl)	EE (%)	S.D.	D.L (%w/w)	S.D.
39	500	**13.45**	0.45	**15.66**	0.53
	1000	**46.19**	5.67	**27.71**	3.40
	1500	**58.14**	2.49	**21.32**	0.91
474	500	**0**	-	**0**	-
	1000	**33.16**	5.51	**27.35**	4.54
	1500	**49.99**	3.56	**23.57**	1.68

Different volumes of TPP were used for each chitosan molecular weight in order to study the influence of this parameter in Doxorubicin loading in chitosan nanoparticles. For the samples using 39 kDa chitosan molecular weight, it can be seen that for 500 µl of TPP correspond an EE of 13%, for 1000 µl of TPP correspond an EE of 46% and for 1500 µl of TPP correspond an EE of 58%. Considering the drug loading, the values obtained were 16%, 28% and 21% for the same samples respectively.

Taking into account the samples using 474 kDa chitosan molecular weight, the EE obtained was 0%, 33% and 50% for 500, 1000 and 1500 µl of TPP respectively. Considering drug loading parameter, it was obtained 0%, 27% and 24% for the same previous samples. Note that the EE and drug loading values for 500 µl of TPP are null which means that no doxorubicin were encapsulated. This could be due to insufficient amount of TPP to form nanoparticles and consequently encapsulate doxorubicin.

Despite that, it can be concluded that EE increases with increasing TPP volume for both chitosan molecular weight tested. Considering drug loading results, it can be said that the 1000 µl of TPP are the best volume to obtain the higher mass ratio between Doxorubicin loaded in nanoparticles and the total mass of the nanoparticles considered. Although the Drug Loading values seem to be similar for both chitosan molecular weight and TPP volumes tested, EE are higher for lower chitosan molecular weight -39 kDa.

4.5.2. Evaluation of *in vitro* Doxorubicin Release

After the encapsulation of doxorubicin in the chitosan nanoparticles the next step is to study its release. For different chitosan molecular weight used to produce the nanoparticles, two different temperatures were been tested, room temperature (25ºC) and body temperature (37ºC). In addition to this parameter, different pH were also been tested.

In order to study the influence of pH, for each temperature, a dialysis apparatus were prepared. Thus, inside and outside the membrane it was used two different pH, 7.4 (PBS solution to simulate bloodstream pH) and 4.5 (to simulate lysosomes and endosomes pH).

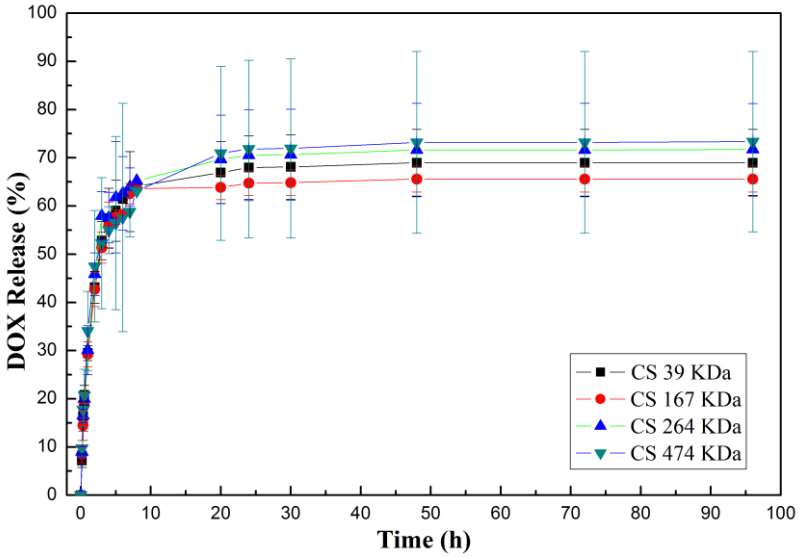

Figure 4.14- Doxorubicin release time study (0-100 h) for room temperature (25ºC) with PBS solution inside and pH 4.5 outside the dialysis membrane.

The first 3 graphs in this section (Figure 4.14, 4.15 and 4.16) are related to the room temperature (25ºC) with different inside and outside membrane pH's solutions. The first one, Figure 4.14, is related to doxorubicin release for PBS 7.4 buffer solution and pH 4.5 inside and outside, respectively. In this

case, it can be seen for all chitosan molecular weight that in the first 10 hours 65% of encapsulated DOX was released. After 20 hours, saturation was reached since the % of DOX release stays the same until the end of this study which means that no DOX was released after that time. However, the DOX release is not equal for all samples. For nanoparticles with higher chitosan molecular weight (474 and 264 kDa) the release was around 70% of the total encapsulated DOX and for nanoparticles with lower molecular weight (167 and 39 kDa) the release was around 65% of the total encapsulated DOX from the dialysis membrane.

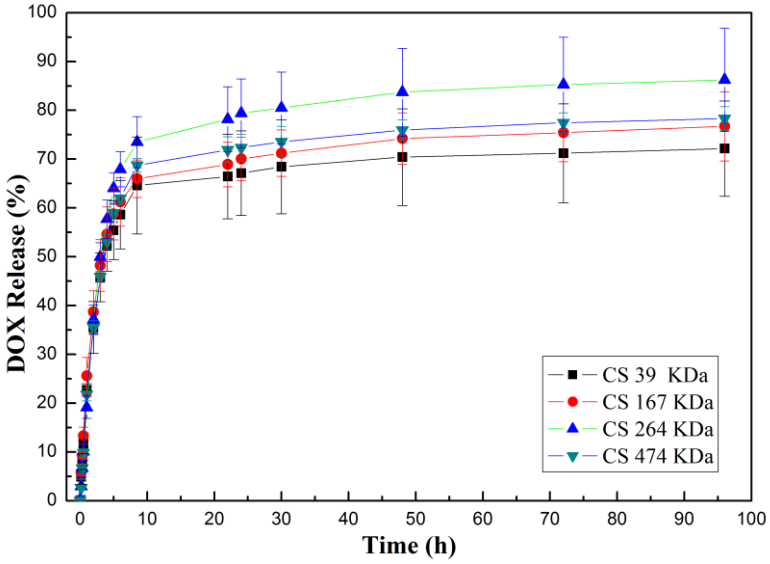

Figure 4.15- Doxorubicin release time study (0-100 h) for room temperature (25ºC) with pH 4.5 inside and PBS solution outside the dialysis membrane.

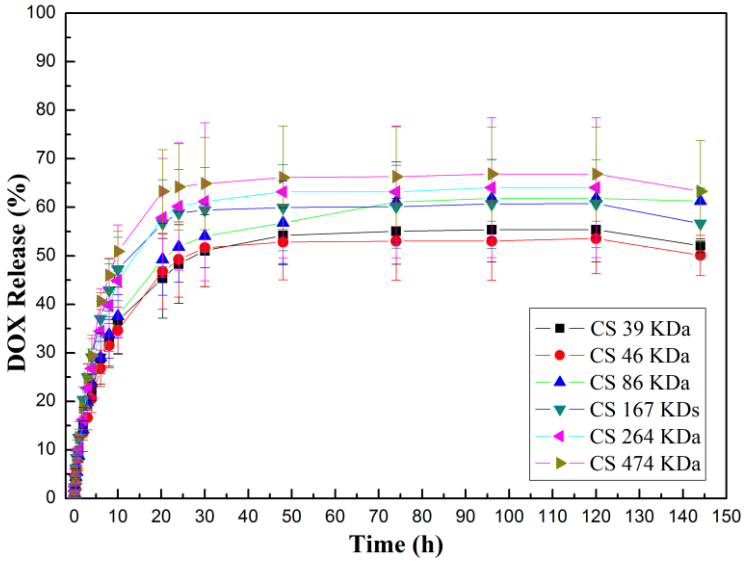

Figure 4.16- Doxorubicin release time study (0-150 h) for room temperature (25ºC) with PBS solution inside and outside the dialysis membrane.

By the analysis of the doxorubicin release graph shown in Figure 4.15, that present pH 4.5 and PBS 7.4 inside and outside the dialysis membrane, respectively, it can be seen that in the first 10 hours 65-75% of encapsulated DOX was released for all the chitosan molecular weight studied. The saturation was reached after 45 hours where around 85% of the total encapsulated DOX was released for the nanoparticles with 264 kDa chitosan molecular weight, 75% was released for the samples using chitosan with 474 and 167 kDa and around 70% was released for the nanoparticles with lower chitosan molecular weight.

The graph represented in Figure 4.16, corresponding to doxorubicin release, PBS 7.4 solution was used inside and outside the membrane. After 30 hours, the saturation was reached for all samples except for the nanoparticles with 86 kDa chitosan that reached saturation around 75 hours. Around 65% of the total encapsulated DOX was released for the nanoparticles with 474 kDa chitosan molecular weight, 60% was released for the samples using chitosan with 264, 167 and 86 kDa and around 55% was released for the nanoparticles with lower chitosan molecular weight (39 and 46 kDa).

The same doxorubicin release time study was made using body temperature (37ºC). The three graphs below shown in Figure 4.17, 4.18 and 4.19 are related to the body temperature with different inside and outside membrane pH's for nanoparticles using different chitosan molecular weight.

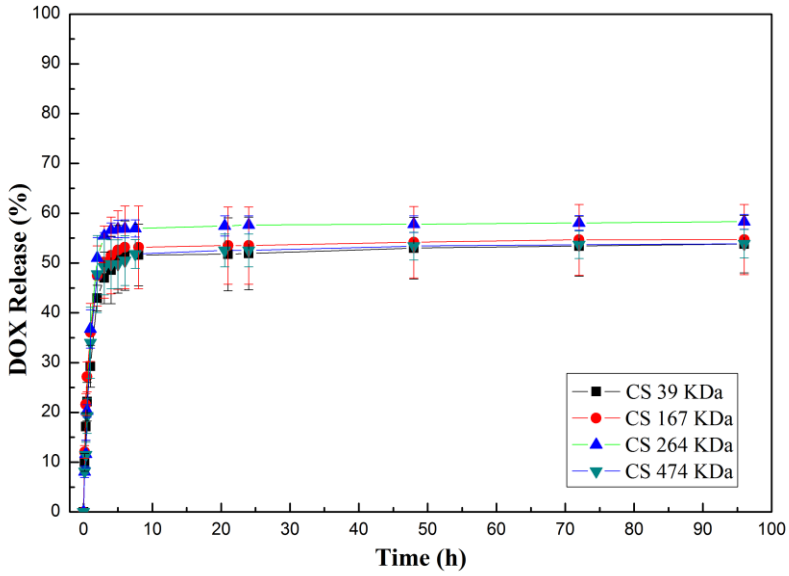

Figure 4.17- Doxorubicin release time study (0-100 h) for body temperature (37ºC) with PBS solution inside and pH 4.5 outside the dialysis membrane.

The first graph related to the body temperature (37ºC) represents the *d*oxorubicin release for PBS solution and pH 4.5 inside and outside the dialysis membrane respectively. As Figure 4.17 suggests after

10 hours, saturation was reached for all the samples. However, the DOX release is not equal for all of them. For nanoparticles with 264 kDa chitosan molecular weight the release was less than 60% of the total encapsulated DOX and for the others nanoparticles (474, 167 and 39 kDa) the release was less than 55% of the total encapsulated DOX from the dialysis membrane.

The next graph related to the body temperature, Figure 4.18, presents the doxorubicin release for pH 4.5 and PBS solution inside and outside the dialysis membrane respectively. After around 5 hours, saturation was reached, but DOX release is not equal for all samples. For nanoparticles with lower chitosan molecular weight, 39 and 167 kDa, the release was around 50% and 45% respectively of the total encapsulated DOX and for nanoparticles with higher molecular weight, 474 and 264 kDa, the release was around 25% of the total encapsulated DOX from the dialysis membrane.

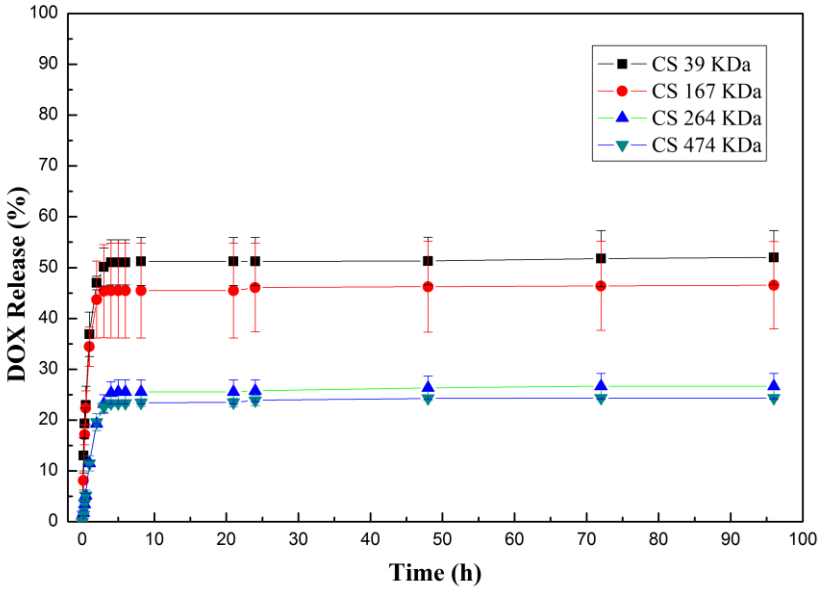

Figure 4.18- Doxorubicin release time study (0-100 h) for body temperature (37ºC) with pH 4.5 inside and PBS solution outside the dialysis membrane

Figure 4.19 presents doxorubicin release for PBS solution used inside and outside the membrane. It can be seen that the saturation was reached after 10 hours. Around 70% of the total encapsulated DOX was released for the nanoparticles with 39 kDa chitosan molecular weight, 65% was released for the samples using chitosan with 474 and 264 kDa and 60% was released for the nanoparticles with 167 kDa chitosan molecular weight.

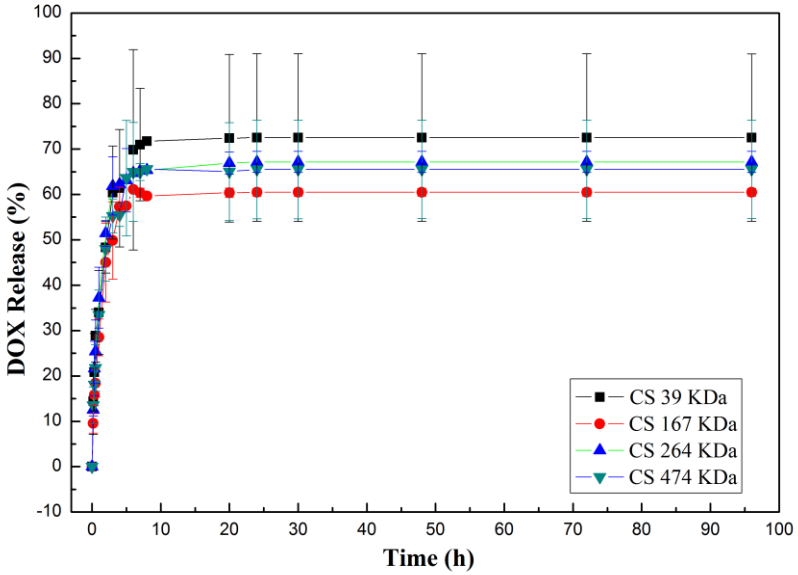

Figure 4.19- Doxorubicin release time study (0-100 h) for body temperature (37ºC) with PBS solution inside and outside the dialysis membrane

After the Doxorubicin release time study results described in this section, it can be concluded that Doxorubicin release behavior is not coherent with the temperature, pH inside and outside the dialysis membrane and chitosan molecular weight used in the nanoparticles produced. Although that, it can be said that the Doxorubicin release level for most samples is around 10 hours of dialysis. No significant differences are verified between the different chitosan molecular weight tested once it cannot be defined a rule between the molecular weight and Doxorubicin release. For room temperature, 25ºC, the sample for pH 4.5 inside the membrane and PBS solution outside the membrane seems to be the best parameters to release more DOX, around of 85% of encapsulated DOX after 45 hours for 264 kDa chitosan nanoparticles. On the other hand, for 37ºC the parameters that suggest a more efficient release are PBS solution in both sides of the membrane, which correspond to a release after 10 hours around 70% of the total encapsulated DOX for the nanoparticles with 39 kDa chitosan.

In order to have more precise results and conclusions it is needed to perform more studies since all this releases are preliminary studies.

4.6. Cytotoxicity studies

Considering that has already been produced and characterized the chitosan, magnetite and chitosan coated iron oxide nanoparticles it is important to study if they are cytotoxic in order to conclude if they are eligible to be used for biomedical applications.

To study the cytotoxicity of synthesized nanoparticles different concentrations of iron were tested in the Fe_3O_4 nanoparticles and different concentrations of chitosan and chitosan coated iron oxide nanoparticles were also tested in Vero cell line.

To characterize the cytotoxicity of the different nanoparticles mentioned above it was used the following criteria:

(i) Severe cytotoxicity: Cellular Viability < 60 %

(ii) Slight cytotoxicity : Cellular Viability between 60-80%

(iii) No cytotoxicity : Cellular Viability > 80%

Figure 4.20 shows the cellular viability of Fe_3O_4 nanoparticles on Vero cells in the range of 0.003-0.4 mg Fe_3O_4 NPs/ml.

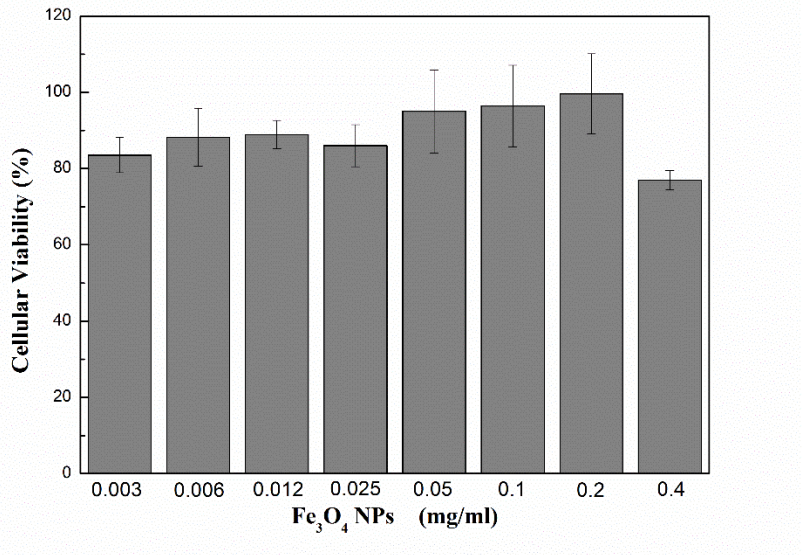

Figure 4.20- Cellular viability of Fe_3O_4 nanoparticles on Vero cell line in the range of 0.003-0.4 mg Fe_3O_4 NPs/ml.

The observation of Figure 4.20 reveals that in the range of 0.003-0.1 mg Fe_3O_4 NPs/ml cellular viability is above 80% on Vero cell line, even taking into account the standard deviation. However, in the 0.4 mg Fe_3O_4 NPs/ml concentration, the cell viability is slightly decreased, less than 80%, which

could be due to mild cytotoxic effect at higher concentrations in the cell line. Thus, it is evident from this study that the magnetite nanoparticles are non-toxic up to the Fe_3O_4 NPs concentration of 0.1 mg/ml on Vero cell line.

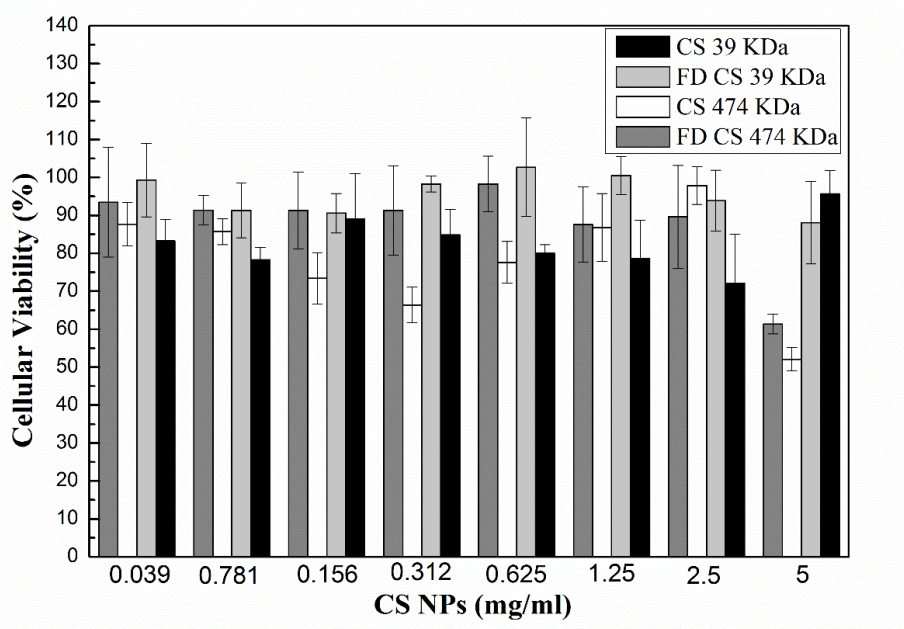

Figure 4.21- Cellular viability of freeze dried (FD) and non-freeze dried Chitosan nanoparticles (39 and 474 kDa) on Vero cell line in the range of 0.039 - 5 mg CS NPs/ml.

Cytotoxicity of chitosan nanoparticles was also studied. Freeze dried and no freeze dried chitosan nanoparticles were tested in different concentrations. Figure 4.21 shows the cellular viability of chitosan nanoparticles on Vero cell line in the range of 0.039-5 mg CS NPs/ml.

Figure 4.21 shows that cellular viability was above 80% for both 39 and 474 kDa freeze dried chitosan nanoparticles in the range of 0.039-5 mg CS NPs/ml which means that these nanoparticles do not show any cytotoxicity on Vero cell line. The exception was the 474 kDa freeze dried chitosan nanoparticles for 5 mg CS NPs/ml that exhibit a cellular viability around 60% which could be due to mild cytotoxic effect at higher concentrations in the cell line.

On the other hand, non-freeze dried chitosan nanoparticles do not exhibit a tendency like the freeze dried nanoparticles referred before. For non-freeze 474 kDa chitosan nanoparticles cellular viability was below 80% for 0.156, 0.312 and 5 mg/ml. Considering the non-freeze 39 kDa chitosan nanoparticles the concentration that shows cellular viability lower than 80% was for 2.5 mg CS NPs/ml. All the other samples exhibit a cellular viability above 80 %, considering standard deviation range, and could be considered non-toxic with Vero cell line.

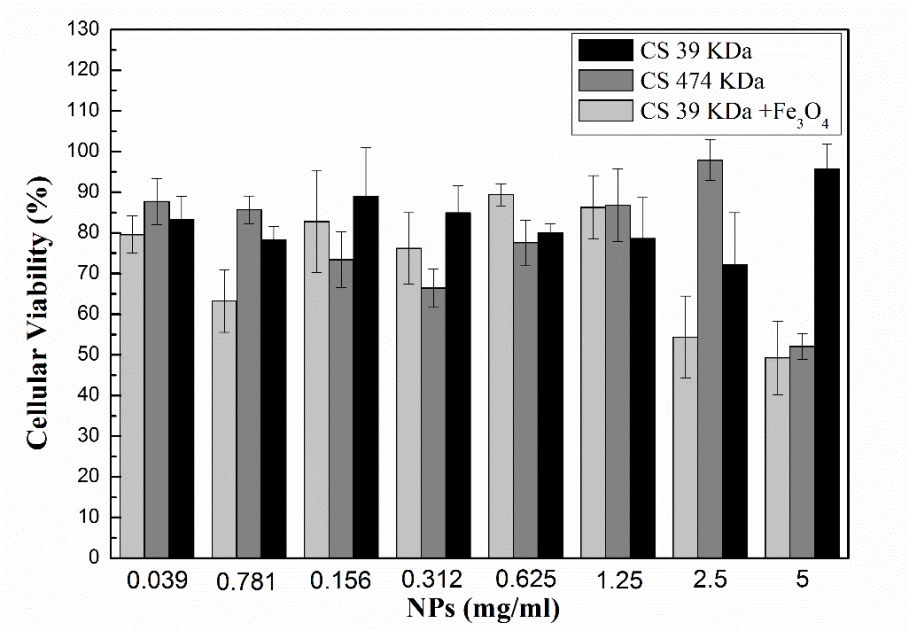

Figure 4.22- Cellular viability of chitosan coated Fe_3O_4 nanoparticles comparing to CS NPs on Vero cell line in the range of 0.03906 – 5 mg NPs/ml.

Finally, after the cytotoxicity studies of iron oxide and chitosan nanoparticles separately, chitosan coated iron oxide nanoparticles were tested in order to study their cytotoxicity on Vero cell line. The observation of Figure 4.22 reveals that chitosan coated magnetite nanoparticles in the range of 0.039-1.25 mg CS SPIONS/ml exhibit a cellular viability above 80%, with the exception of 0.7813 mg/ml, which means that do not show any cytotoxicity in Vero cell line. However, in the 2.5 and 5 mg CS SPIONPs/ml concentration, the cellular viability is decreased slightly, less than 60%, which could be due to mild cytotoxic effect at higher concentrations in the cell line.

In resume, it can be said that, based in this study, the chitosan coated magnetite nanoparticles are non-toxic up to the CS SPIONS concentration of 1.25 mg/ml.

5. CONCLUSIONS

Depolymerization technique proved to be an efficient procedure to decrease the molecular weight of commercial CS (474 kDa) since it was possible to obtained samples between 39 - 474 kDa. FTIR analysis shows that no structural change is notice in those chitosan samples.

Chitosan nanoparticles were obtained by ionic gelation technique and their lowest diameters were around 100 nm calculated by DLS measurements. For each chitosan molecular weight was used three different pH (5, 9, and 13) with and without magnetic stirring. The present work shows that the chitosan nanoparticles diameters increases with increasing chitosan molecular weight, but there are not significant differences between pH 5, 9, and 13 with the exception of pH 13 in the higher chitosan molecular weight (264 and 474 kDa). In some cases the nanoparticles diameters with magnetic stirring were smaller than the others.

Turrax equipment was used, as an alternative of magnetic stirring, and although the diameters are similar to those obtained previously, the standard deviation is much smaller compared to the ones obtained with magnetic stirring. Another relevant aspect is that the *Turrax* is faster than magnetic stirring, as can be obtained nanoparticles with the same diameter with only 5 minutes instead of 24 hours of agitation. FTIR studies confirm the presence of chitosan in chitosan nanoparticles formed by ionic gelation technique.

Fe_3O_4 nanoparticles were obtained by thermal decomposition. X-ray diffraction was performed to associate these nanoparticles with magnetite. TEM analysis shows that these nanoparticles present a roughly spherical morphology and were not bonded. The particle size was determined by statistical analysis of the dimensions of at least 100 particles yielding an average particle diameter of 10.3 ± 2.0 nm (TEM) and 13.54 nm (XRD). These Fe_3O_4 nanoparticles synthesized possess the ability to generate heat. The heating ability of this nanoparticles rises with increasing iron concentration as it was shown by Hyperthermia studies. SQUID measurements indicate the superparamagnetic behavior of Fe_3O_4 nanoparticles at room temperature – 315 K.

The main goal of the present work was to join the two previously synthesized nanoparticles in order to produce chitosan coated iron oxide nanoparticles. pH 13 seems to be the best pH to be used and magnetic stirring gives smaller diameters. On the other hand, CS/SPIONs ratio depends on which chitosan molecular weight is being used. The smaller diameter was obtained for CS 46 kDa, pH13 without magnetic stirring and 2-1 CS/SPIONs ratio. Should be noted that the standard deviation are relatively large in some samples. FTIR analysis indicate that the chitosan coating is present on the SPIONs surface.

Chitosan coated Fe_3O_4 nanoparticles synthesized possess the ability to generate heat. It can be seen that the heating ability of this nanoparticles rises with decreasing TPP volumes. In fact, when the volume of TPP is increased chitosan crosslinking increases which leads to a decrease in the heat generating ability of this nanoparticles. Higher iron concentrations correspond to higher heating efficiencies of the chitosan coated Fe_3O_4 nanoparticles as well as it was seen for Fe_3O_4 nanoparticles. SQUID measurements indicate the superparamagnetic behavior of chitosan coated Fe_3O_4 nanoparticles at room temperature – 315 K.

Doxorubicin loading studies show that Encapsulation Efficiency (EE) increases with increasing TPP volume. Considering Drug Loading results, it can be said that the 1000 µl of TPP are the best volume to obtain the higher mass ratio between Doxorubicin loaded in nanoparticles and the total mass of the nanoparticles considered. Although the Drug Loading values seem to be similar for both chitosan molecular weight (39 and 474 kDa) and TPP volumes tested, EE are higher for lower chitosan molecular weight.

In vitro release studies show that the majority of Doxorubicin is released in the first 10-20 hours of dialysis. No significant differences are verified between the different chitosan molecular weight tested once it cannot be defined a rule between the molecular weight and Doxorubicin release. For room temperature, 25ºC, the sample for pH 4.5 inside the membrane and PBS solution outside the membrane seems to be the best parameters to release more DOX, around of 85% of encapsulated DOX after 45 hours for 264 kDa chitosan nanoparticles. On the other hand, for 37ºC the parameters that suggest a more efficient release are PBS solution in both sides of the membrane, which correspond to a release after 10 hours around 70% of the total encapsulated DOX for the nanoparticles with 39 kDa chitosan. It can be concluded that the release is higher and slower for 25ºC comparing to 37ºC.

This work shows that magnetite nanoparticles do not show any cytotoxicity with Vero cell line in the range of 0.003 - 0.1 mg Fe_3O_4 NPs/ml. However, in the 0.4 mg Fe_3O_4 NPs/ml concentration, the cell viability is decreased slightly (less than 80%) which could be due to mild cytotoxic effect at higher concentrations in the cell line. Thus, it is evident from this study that the magnetite nanoparticles are non-toxic up to the Fe_3O_4 NPs concentration of 0.1 mg/ml. It can be also said, from this study, that the chitosan coated magnetite nanoparticles are non-toxic up to the CS SPIONS concentration of 1.25 mg/ml.

All the studies made in the present work, besides they are preliminary, show that chitosan coated iron oxide nanoparticles could be used for biomedical applications.

REFERENCES

1. Amaneh Javid, S.A., Ali Akbar Saboury, Seyed Mehdi Kalantar, Sughra Shahzad, and Saeed Rezaei-Zarchi, *Synthesis and Characterization of Chitosan-Modified Doxorubicin-Loaded Iron Oxide Nanoparticles.* International Conference on Ecological, Environmental and Biological Sciences, 2012: p. 438-442.
2. Heidel, J.D. and M.E. Davis, *Clinical developments in nanotechnology for cancer therapy.* Pharm Res, 2011. **28**(2): p. 187-99.
3. Javid, A., et al., *Chitosan-coated superparamagnetic iron oxide nanoparticles for doxorubicin delivery: synthesis and anticancer effect against human ovarian cancer cells.* Chem Biol Drug Des, 2013. **82**(3): p. 296-306.
4. Ana Baptista, P.S., Isabel Ferreira, and João Paulo Borges, *Bioengineered nanomaterials,* in A.T.a.A. Tiwari, Editor. 2013, CRC Press Taylor & Francis Group p. 93-117.
5. Kreyling, W.G., M. Semmler-Behnke, and Q. Chaudhry, *A complementary definition of nanomaterial.* Nano Today, 2010. **5**(3): p. 165-168.
6. Bleeker, E.A., et al., *Considerations on the EU definition of a nanomaterial: science to support policy making.* Regul Toxicol Pharmacol, 2013. **65**(1): p. 119-25.
7. Lee, C.M., et al., *SPION-loaded chitosan-linoleic acid nanoparticles to target hepatocytes.* Int J Pharm, 2009. **371**(1-2): p. 163-9.
8. Maity, D., et al., *Synthesis of Hydrophilic Superparamagnetic Magnetite Nanoparticles via Thermal Decomposition of Fe(acac)3 in 80 Vol% TREG + 20 Vol% TREM.* Journal of Nanoscience and Nanotechnology, 2011. **11**(3): p. 2730-2734.
9. DONGWON YOO, J.-H.L., TAE-HYUN SHIN, AND and J. CHEON*, *Theranostic Magnetic Nanoparticles.* Accounts of chemical research 2011. **44**: p. 863-874.
10. TWAN LAMMERS, S.A., WIM E. HENNINK, and A.F.K. GERT STORM, *Theranostic Nanomedicine.* ACCOUNTS OF CHEMICAL RESEARCH, 2011. **44**: p. 1029–1038.
11. *Nanoparticles in Biomedical Imaging*. Springer ed. Emerging Technologies and Applications. 2008.
12. Park, B.-H., et al., *Comparison of labeling efficiency of different magnetic nanoparticles into stem cell.* Colloids and Surfaces A: Physicochemical and Engineering Aspects, 2008. **313-314**: p. 145-149.
13. Grootendorst, D.J., et al., *Evaluation of superparamagnetic iron oxide nanoparticles (Endorem(R)) as a photoacoustic contrast agent for intra-operative nodal staging.* Contrast Media Mol Imaging, 2013. **8**(1): p. 83-91.
14. W. Hundt, R.P., T. Helmberger, M. Reiser, *Signal changes in liver and spleen after Endorem administration in patients with and without liver cirrhosis.* European Radiology, 2000. **10**: p. 409-416.
15. Bonnemain, B., *Pharmacokinetic and Hemodynamic Safety of Two Superparamagnetic Agents, Endorem and Sinerem, in Cirrhotic Rats.* Academy Radiology 1998. **5**: p. 151-153.
16. Lunov, O., et al., *Lysosomal degradation of the carboxydextran shell of coated superparamagnetic iron oxide nanoparticles and the fate of professional phagocytes.* Biomaterials, 2010. **31**(34): p. 9015-22.
17. Kemp H. Kernstine, W.S., Brian F. Mullan,, B.H.T. Nicholas P. Rossi, David L. Bushnell,, and a.J.A.K. Kelley A. McLaughlin, *PET, CT, and MRI With Combidex for*

Mediastinal Staging in Non-Small Cell Lung Carcinoma. The Society of Thoracic Surgeons, 1999. **68**: p. 1022-1028.
18. Mukesh G Harisinghani, S.S., Gregory J. Slater, Mitchell D. Schnall, Matthew D. Rifkin, , *MR Imaging of Pelvic Lymph Nodes in Primq-Pelvic Carcinoma-with Ultrasmall Superparamagnetic Iron Oxide (Combidex): Preliminary Observations.* Journal of Magnetic Resonance Imaging, 1997. **7**: p. 161-63.
19. Xu, Q., et al., *In vitro and in vivo magnetic resonance tracking of Sinerem-labeled human umbilical mesenchymal stromal cell-derived Schwann cells.* Cell Mol Neurobiol, 2011. **31**(3): p. 365-75.
20. Sigal, R., et al., *Lymph node metastases from head and neck squamous cell carcinoma: MR imaging with ultrasmall superparamagnetic iron oxide particles (Sinerem MR) -- results of a phase-III multicenter clinical trial.* Eur Radiol, 2002. **12**(5): p. 1104-13.
21. Qiu, D., et al., *Contrast-enhanced functional blood volume imaging (CE-fBVI): enhanced sensitivity for brain activation in humans using the ultrasmall superparamagnetic iron oxide agent ferumoxytol.* Neuroimage, 2012. **62**(3): p. 1726-31.
22. D'Arceuil, H., et al., *Ferumoxytol enhanced resting state fMRI and relative cerebral blood volume mapping in normal human brain.* Neuroimage, 2013. **83**: p. 200-9.
23. Bravo, S.M., et al., *Safety and Efficacy of Ferumoxytol as a Lymphatic Contrast Agent.* International Journal of Radiation Oncology*Biology*Physics, 2013. **87**(2): p. S171-S172.
24. Siegers, G.M., et al., *Extensive expansion of primary human gamma delta T cells generates cytotoxic effector memory cells that can be labeled with Feraheme for cellular MRI.* Cancer Immunol Immunother, 2013. **62**(3): p. 571-83.
25. Steve Chaplin BPharm, M.a.M.B.P., MRCP, *Ferumoxytol (Rienso): new intravenous iron preparation.* 2013.
26. Lodhia, J., et al., *Development and use of iron oxide nanoparticles (Part 1): Synthesis of iron oxide nanoparticles for MRI.* Biomed Imaging Interv J, 2010. **6**(2): p. e12.
27. Damasceno, B.P.G.L.S., J.A.; Oliveira, E.E.; Silveira, W.L.L.; Araújo, I.B; Oliveira,A.G.; Egito, E.S.T.; , *Microemulsão: um promissor carreador para moléculas insolúveis.* Rev. Ciênc. Farm. Apl., , 2011. **32**: p. 9-18.
28. Lin, M.M.K., D.K.; Haj, A. J. E.; Dobson, J.; , *Development of superparamagnetic iron oxide nanoparticles (SPIONS) for translation clinical applications.* IEEE Transactions on nanobioscience, 2008. **7**: p. 298-305.
29. Pérez, J.A.L.Q., M. A. L.; Mira, J.; Rivas, J.;, *Preparation of magnetic fluids with particles obtained in microemulsion.* IEEE Transactions on Magnetics 1997. **33**(5): p. 4359-4362.
30. Maity, D., et al., *Studies of magnetite nanoparticles synthesized by thermal decomposition of iron (III) acetylacetonate in tri(ethylene glycol).* Journal of Magnetism and Magnetic Materials, 2009. **321**(19): p. 3093-3098.
31. Miguel-Sancho, N., et al., *Development of Stable, Water-Dispersible, and Biofunctionalizable Superparamagnetic Iron Oxide Nanoparticles.* Chemistry of Materials, 2011. **23**(11): p. 2795-2802.
32. Rinaudo, M., *Chitin and chitosan: Properties and applications.* Progress in Polymer Science, 2006. **31**(7): p. 603-632.
33. Kumar, M.N.V.R., *A review of chitin and chitosan applications.* Reactive & Functional Polymers, 2000. **46**: p. 1-27.

34. Kevin A. Janes , M.P.F., Ana Marazuela , Angels Fabra , and M.J. Alonso, *Chitosan nanoparticles as delivery systems for doxorubicin.* Journal of Controlled Release, 2001. **73**: p. 255-267.
35. Tan, M.L., P.F. Choong, and C.R. Dass, *Review: doxorubicin delivery systems based on chitosan for cancer therapy.* J Pharm Pharmacol, 2009. **61**(2): p. 131-42.
36. Li, P., et al., *Development of chitosan nanoparticles as drug delivery systems for 5-fluorouracil and leucovorin blends.* Carbohydr Polym, 2011. **85**(3): p. 698-704.
37. Bu, L., et al., *Trans-resveratrol loaded chitosan nanoparticles modified with biotin and avidin to target hepatic carcinoma.* Int J Pharm, 2013. **452**(1-2): p. 355-62.
38. Jiang, M., et al., *Cationic core-shell liponanoparticles for ocular gene delivery.* Biomaterials, 2012. **33**(30): p. 7621-30.
39. Csaba, N., M. Koping-Hoggard, and M.J. Alonso, *Ionically crosslinked chitosan/tripolyphosphate nanoparticles for oligonucleotide and plasmid DNA delivery.* Int J Pharm, 2009. **382**(1-2): p. 205-14.
40. Katas, H. and H.O. Alpar, *Development and characterisation of chitosan nanoparticles for siRNA delivery.* J Control Release, 2006. **115**(2): p. 216-25.
41. Alishahi, A., et al., *Shelf life and delivery enhancement of vitamin C using chitosan nanoparticles.* Food Chemistry, 2011. **126**(3): p. 935-940.
42. Khatri, K., et al., *Plasmid DNA loaded chitosan nanoparticles for nasal mucosal immunization against hepatitis B.* Int J Pharm, 2008. **354**(1-2): p. 235-41.
43. Sonaje, K., et al., *Effects of chitosan-nanoparticle-mediated tight junction opening on the oral absorption of endotoxins.* Biomaterials, 2011. **32**(33): p. 8712-21.
44. Yan Pan, Y.-j.L., Hui-ying Zhao, Jun-min Zheng, Hui Xu, and J.-s.H. Gang Wei, Fu-de Cui *Bioadhesive polysaccharide in protein delivery system:chitosan nanoparticles improve the intestinal absorption of insulin in vivo.* International Journal of Pharmaceutics, 2002. **249**: p. 139-147.
45. Gan, Q. and T. Wang, *Chitosan nanoparticle as protein delivery carrier--systematic examination of fabrication conditions for efficient loading and release.* Colloids Surf B Biointerfaces, 2007. **59**(1): p. 24-34.
46. Dudhani, A.R. and S.L. Kosaraju, *Bioadhesive chitosan nanoparticles: Preparation and characterization.* Carbohydr Polym, 2010. **81**(2): p. 243-251.
47. Zhang, L. and S.L. Kosaraju, *Biopolymeric delivery system for controlled release of polyphenolic antioxidants.* European Polymer Journal, 2007. **43**(7): p. 2956-2966.
48. Dube, A., J.A. Nicolazzo, and I. Larson, *Chitosan nanoparticles enhance the intestinal absorption of the green tea catechins (+)-catechin and (-)-epigallocatechin gallate.* Eur J Pharm Sci, 2010. **41**(2): p. 219-25.
49. Kouachi, *Potential Applications of Chitosan Nanoparticles as Novel Support in Enzyme Immobilization.* American Journal of Biochemistry and Biotechnology, 2012. **8**(4): p. 203-219.
50. Qi, L., et al., *Preparation and antibacterial activity of chitosan nanoparticles.* Carbohydr Res, 2004. **339**(16): p. 2693-700.
51. Dong, Y., et al., *Scalable ionic gelation synthesis of chitosan nanoparticles for drug delivery in static mixers.* Carbohydr Polym, 2013. **94**(2): p. 940-5.
52. Tiyaboonchai, W., *Chitosan Nanoparticles :A Promising System for Drug Delivery* Naresuan University Journal, 2003. **11**(3): p. 51-66.
53. Agnihotri, S.A., N.N. Mallikarjuna, and T.M. Aminabhavi, *Recent advances on chitosan-based micro- and nanoparticles in drug delivery.* J Control Release, 2004. **100**(1): p. 5-28.

54. Songsurang, K., et al., *Electrospray fabrication of doxorubicin-chitosan-tripolyphosphate nanoparticles for delivery of doxorubicin.* Arch Pharm Res, 2011. **34**(4): p. 583-92.
55. Zheng, A.-p., et al., *Comprehensive studies on the interactions between chitosan nanoparticles and some live cells.* Journal of Nanoparticle Research, 2011. **13**(10): p. 4765-4776.
56. S. Mitraa, U.G., P.C. Ghosha, A.N. Maitrab, *Tumour targeted delivery of encapsulated dextran-doxorubicin conjugate using chitosan nanoparticles as carrier.* Journal of Controlled Release, 2001. **74**: p. 317-323.
57. Barenholz, Y., *Doxil(R)--the first FDA-approved nano-drug: lessons learned.* J Control Release, 2012. **160**(2): p. 117-34.
58. Zhao, Y., et al., *A simple way to enhance Doxil(R) therapy: drug release from liposomes at the tumor site by amphiphilic block copolymer.* J Control Release, 2013. **168**(1): p. 61-9.
59. Kasaai, M.R., *Calculation of Mark-Houwink-Sakurada (MHS) equation viscometric constants for chitosan in any solvent-temperature system using experimental reported viscometric constants data.* Carbohydrate Polymers, 2007. **68**: p. 477-488.
60. Kasaai, M.R., *Calculation of Mark–Houwink–Sakurada (MHS) equation viscometric constants for chitosan in any solvent–temperature system using experimental reported viscometric constants data.* Carbohydrate Polymers, 2007. **68**(3): p. 477-488.
61. Marina Talelli, C.J.F.R., Twan Lammers, Peter R. Seevinck, and C.F.v.N. Gert Storm, and Wim E. Hennink, *Superparamagnetic Iron Oxide Nanoparticles Encapsulated in Biodegradable Thermosensitive Polymeric Micelles: Toward a Targeted Nanomedicine Suitable for Image-Guided Drug Delivery.* American Chemical Society, 2009. **25**(4): p. 2060-2067.
62. Chilukuri S.P. Sastry , J.S.V.M.L.R., *Determination of doxorubicin hydrochloride by visible spectrophotometry.* Talanta, 1996. **43**: p. 1827-1835.
63. Mohammadpour Dounighi N, e.a., *Preparation and in vitro characterization of chitosan nanoparticles containing Mesobuthus eupeus scorpion venon as an antigen delivery system.* Mesobuthus eupeus scorpion venon and nanoparticle compounds J Venom Anim Toxins incl Trop Dis, 2012. **18**(1): p. 48.
64. Zhang, W.J., S.; Wu, Q.; Ran, J.; Liu, Y.; Hou, J.;, *Studies of the magnetic field intensity on the synthesis of chitosan-coated magnetite nanocomposites by co-precipitation method.* Materials Science and Engineering 2012. **32**: p. 381-384.
65. Wu, S.S., A.; Zhai, F.; Wang, J.; Xu, W.; Zhang, Q; Volinsky, A.;, *Fe3O4 magnetic nanoparticles synthesis from talings by ultrasonic chemical co-precipitation.* Materials Letters 2011. **65**: p. 1882-1884.
66. Kallumadil, M.T., M.; Nakagawa, T.; Abe, M.; Southern, P.; Pankhurst, Q.;, *Suitability of commercial colloids for magnetic hyperthermia.* Journal of Magnetism and Magnetic Materials, 2009. **321**: p. 1509-1513.
67. Unsy, G.Y., S.; Khodadust, R.; Gunduz, G.; Gunduz, U.; , *Synthesis optimization and characterization of chitosan-coated iron oxide nanoparticles produced for biomedicals applications* Journal of Nanoparticle Research, 2012. **14**.